Molecular and Nano-engineering with iron, ruthenium and carbon: Hybrid structures for sensing

Geest, E.P. van

Appendix

Chapter 2

Materials and methods for device fabrication

Bapbpy was synthesized using a previously reported protocol.[1] Single crystals of Fe(bapbpy)$(NCS)_2$ were prepared using a liquid-liquid diffusion method developed in our group.[2] Shortly, a solution of $Fe(SCN)_2$ in degassed methanol (0.1 M, 0.17 ml) was carefully layered on top of a solution of bapbpy in DMF (1.5 mM, 1.0 ml, filtrated before use) in a 15 ml corning tube containing two vertically positioned silica wafers (Prime grade, 285 nm SiO_2 on 0.5 mm Si, single side polished; approx. 8x8 mm in size; functionalized with trimethoxyoctadecyl silane (OTMS). Silanization was done on cleaned wafers (sonication in acetone, MilliQ and isopropanol, then O_2 plasma: 0.30 mbar, 100 W, 2 minutes) by immersing them in a 1% OTMS solution in hexane, overnight at room temperature, then rinsing them with hexane, toluene, ethanol and MilliQ. The wafers were positioned at the DMF-methanol interface in the crystallization tube for crystal growth on the polished silicon oxide surface. On top of the $Fe(SCN)_2$ layer, an excess of methanol (7 ml, degassed by nitrogen bubbling) was carefully layered to not disturb the DMF-methanol interface. After 3 days, methanol was diffused into the DMF layer and single crystals had grown on the silica wafers and the tube walls. The crystallization liquid was removed and wafers were rinsed thoroughly with methanol thrice, then left to dry on air.

Graphene transistors on SCO single crystals were fabricated on single crystals that were grown on the wafers. Full wafers were cast in a flexible epoxy film (Reprorubber Thin Pour, film thickness 0.15 ± 0.02 mm) which was extracted from the wafer carefully, to avoid damaging the crystals. Wafers were functionalized with OTMS beforehand to decrease the affinity of the epoxy film for the wafer surface. From the epoxy sheet, turned upside down with crystals facing upwards, individual crystals (with parallelogram-shaped surface) were selected and transferred together with their epoxy matrix by mechanical cutting, the epoxy film with one crystal was placed on a thin glass slide (0.15 ± 0.02 mm) with the crystal facing up, and fixed to the slide using little of the flexible epoxy resin. Once cured, excess resin was removed (as close as possible to the acute corners of the crystal, at an 90° angle with the long sides of the crystal surface), leaving the crystal on a strip of epoxy resin.

For devices with a spacer, a poly(methyl methacrylate) (PMMA) film was spin-coated on copper foil; spacer thickness varied with rotation speed (6000 rpm = 0.1 μm, 4000 rpm = 0.3 μm, 1000 rpm = 0.5 μm). Copper was then etched with an ammonium persulfate solution (0.2 M in MilliQ), the film was rinsed by transferring the sheet in three MilliQ baths consecutively, then transferred on the crystal by fishing the floating film from below. The unfinished device was then heated at 120°C for 1 hour. Next, electrically conductive silver epoxy (Gentec, EPOTEK EJ2189-LV) was manually placed next to the long edges of the crystal surface, as close as possible to the crystal, without touching (the electrodes did not physically touch the substrate crystal to prevent mechanical effects of the electrodes during cooling or heating). Copper wires were attached to the silver epoxy electrodes and the epoxy was allowed to cure overnight at room temperature.

A piece of PMMA-coated graphene (grown by chemical vapor deposition (CVD), monolayer on copper foil; purchased from Graphenea or grown in-house in a CVD tube oven), spin-coated with PMMA (6% in anisole, Allresist GmbH., AR-P 662.06; 4000 rpm for 60 s, heated at 85°C for 10 minutes, then back-etched in oxygen plasma (0.30 mbar, 100 W, 2 minutes) was transferred using the same method as the PMMA spacer (see above). The sheet was transferred to the crystal and silver epoxy electrodes by fishing from below with the unfinished device. Excess water was removed with soft tissue and the device was heated at 120°C for at least 1 hour. Excess graphene was removed

mechanically using a razor blade, leaving the graphene on and between the silver epoxy electrodes intact, to finish the device (see Figure S2.1).

For devices with a gate electrode, the same procedure was followed, however the graphene transferring polymer was slightly different; instead of spin-coating the PMMA solution as received, 2wt% of the ionic liquid DEME-TFSI, where DEME-TFSI = N,N-diethyl-N-methyl-N-(2-methoxyethyl)ammonium bis(trifluoromethanesulfonyl)imide, was premixed with the PMMA solution to form a PMMA/DEME-TFSI hybrid film on top of graphene. The introduction of DEME-TFSI did not influence the graphene etching and transfer step or any of the following fabrication steps. After the graphene transfer, devices were treated with O_2 plasma (0.30 mbar, 100 W, 1 minute), then the source and drain electrodes were protected with Reprorubber epoxy resin (see Figure S2.2B). Next, a piece of copper foil was cut into a sharp tip with a large base for electrical connection of the gate electrode. The far end of the tip was placed above the crystal, then the copper foil electrode was locked in place with Reprorubber epoxy and a droplet of ionic liquid was carefully placed between the protected electrodes and on top of the crystal (the size of the droplet was as such that the full area was covered without overflowing) to complete the gated graphene field effect transistor (see Figure S2.1).

Oxygen plasma was generated using a capacitively coupled plasma system with radio-frequency of 40 kHz and 200 W power from Diener electronic (Femto), employed at room temperature. Spin coating was done with a POLOS SPIN150i tabletop spin coater. Optical images were obtained using a Leica DM2700 M Brightfield microscope fitted with Leica MC120 HD camera. AFM images were recorded on a JPK Nanowizard Ultra. Magnetic measurements were performed using a Quantum Design MPMS XL SQUID Magnetometer. Raman spectra were recorded on a Witec Alpha500 R Raman spectrometer using a 532 nm laser at low power (0.23 mW). Electrical characterization of devices was performed using a Keithley Sourcemeter model 2450 and 2400 in combination with Kickstart measuring software. Gate voltage (for top-gated devices) was supplied using a Keithley Sourcemeter (model 2400) while measuring resistance with a separate Keithley Sourcemeter (model 2450), both earthed on the same point. Optical footage of the device inside the chamber was recorded using the optical camera equipped to the Raman microscope setup. Temperature cycling experiments were performed using a Linkam THMS600E microscope heating/cooling stage equipped on the Raman spectrometer in combination with LINK temperature control software. During temperature cycle experiments, the devices were electrically connected inside the heating/cooling stage. To prevent condensation, the chamber was purged with N_2 (N3.0 or higher) at the start each experiment, according to the manufacturer's protocol.

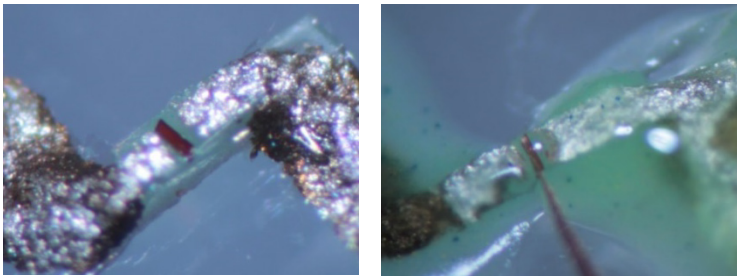

Figure S2.1: Finished graphene transistor constructed on spin crossover crystal without gate electrode (left) and with gate electrode (right).

Schematic representation of fabrication step-by-step

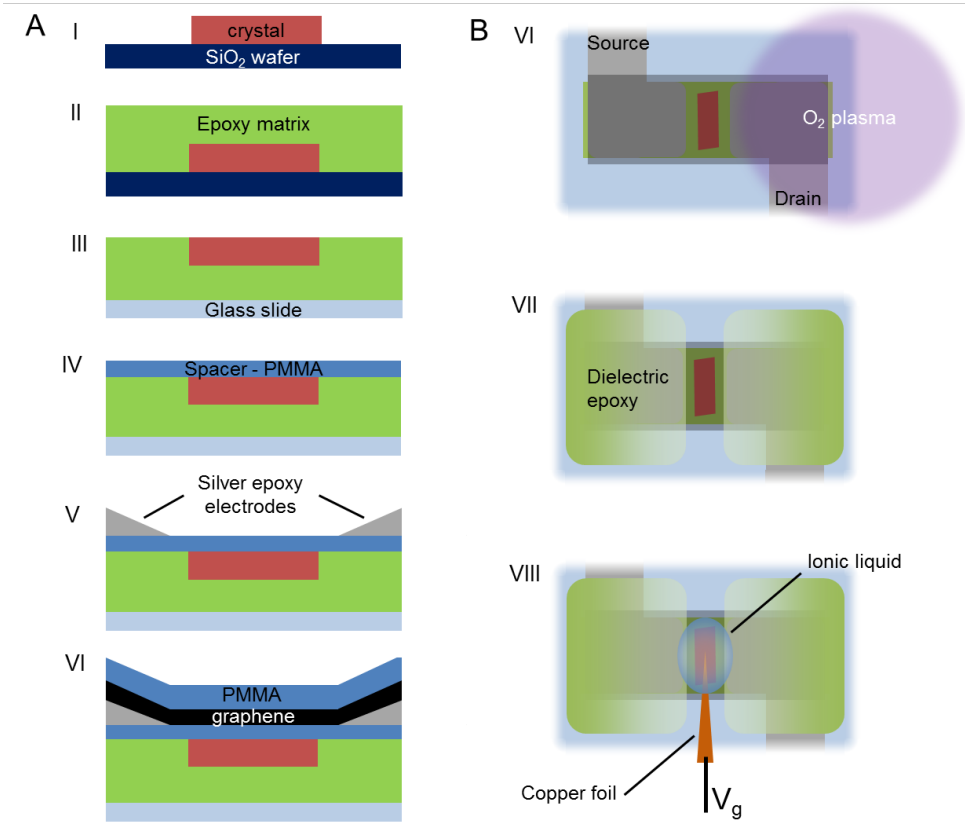

Figure S2.2: A) Side view step-by-step schematic representation of the production process of graphene transistors on SCO crystals. I: Single crystal of **1** grown on Si/SiO2 wafer; II: crystal on wafer cast in epoxy resin; III: epoxy, holding crystal pulled from wafer and placed upside down on a microscope cover glass; IV: PMMA film transferred onto the epoxy and the crystal; V: solid silver epoxy electrodes placed close to crystal edges; VI: transfer of a PMMA-graphene film (graphene below; for gated devices a premixed PMMA/DEME-TFSI film was used for graphene transfer) and mechanical removal of excess graphene to finish the device. B) VI: Top-side view of finished device – for gating, the devices were subjected to oxygen plasma; VII: protection of source and drain electrodes with dielectric epoxy resin; VIII: construction of gate electrode from copper foil and placement of ionic liquid DEME-TFSI on the crystal area for gating experiments.

Graphene characterization by AFM and Raman spectroscopy

AFM images of the surface of a typical crystal on a wafer showed a particularly smooth and clean surface of a bare crystal (see Figure S2.3A). Notably, micrometer-sized terraces and trenches were identified with step sizes of about 1 nm, *i.e.* single molecule thickness. After transferring graphene and removing the carrier polymer, the surface topology was wave-like, indicative of an intact, slightly

wrinkled graphene sheet on top of the crystal (see Figure S2.3B). The deposits on the surface were likely remains of PMMA after the transfer. Raman spectra of coated crystals showed the 2D peak at 2705 cm^{-1} typical for graphene, while it was not present for uncoated crystals (see Figure S2.3C). A line scan showed that the presence of graphene is continuous (see Figure S2.3C, inset). Moreover, a peak indicative of structural defects in graphene, typically observed near 1350 cm^{-1}, was not observed. Thus, graphene was successfully transferred on the single crystal of **1** and was of high quality.

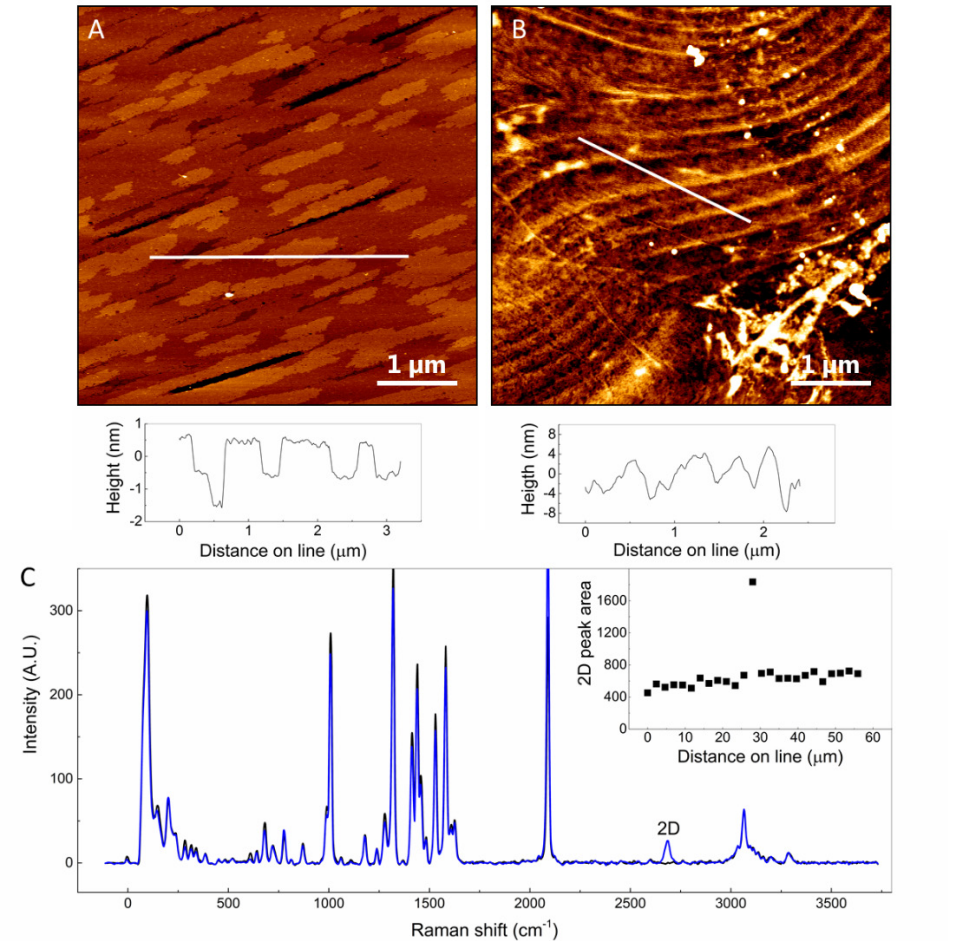

Figure S2.3: AFM images of an uncoated (A) and graphene-coated (B) single crystal of compound **1** (PMMA removed after graphene transfer) and corresponding height profiles. C) Raman spectrum of the uncoated (black) and coated (blue) single crystal of **1**, showing the 2D peak typical for graphene at 2700 cm^{-1} for the coated crystal. Inset: a line scan across the coated crystal shows continuous presence of graphene, *i.e.* the 2D peak, at the crystal surface. NB: the elevated point is considered an artefact (*i.e.* a wrinkle in graphene).

Resistance measurements for low-temperature phase II to phase III transitions

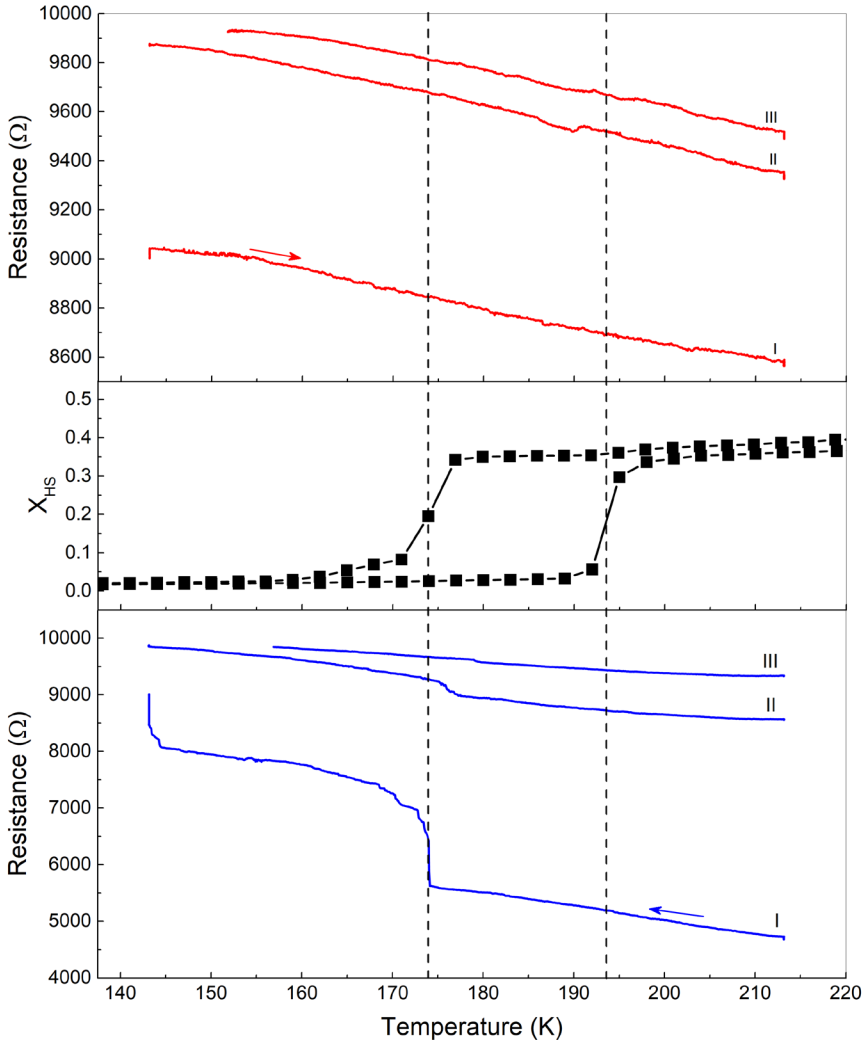

Figure S2.4: Resistance (red = heating mode, blue = cooling mode) and single crystal high-spin fraction x_{HS} (connected black squares) *vs.* temperature for a device with 0.5 μm spacer. Dashed lines indicate transition temperatures. The number of the cooling-heating cycle is denoted with I, II and III.

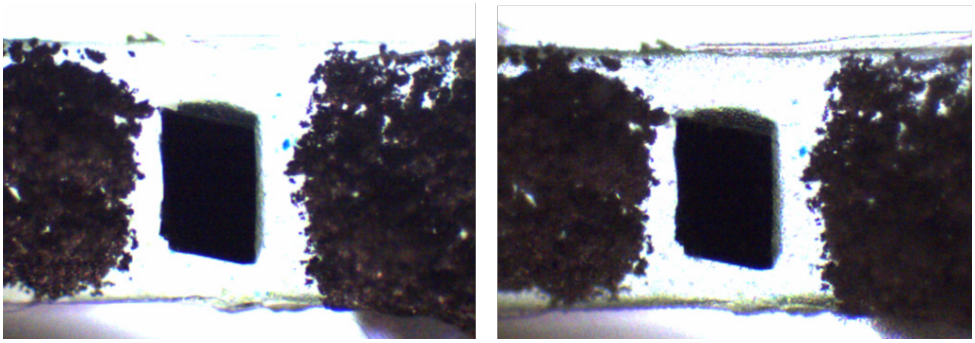

Figure S2.5: Optical image of a spin crossover crystal (in a device) in phase II (left) and in phase III (right). Crystal length and width are 225 μm and 160 μm.

Mechanical resilience to multiple temperature-induced spin crossover cycles

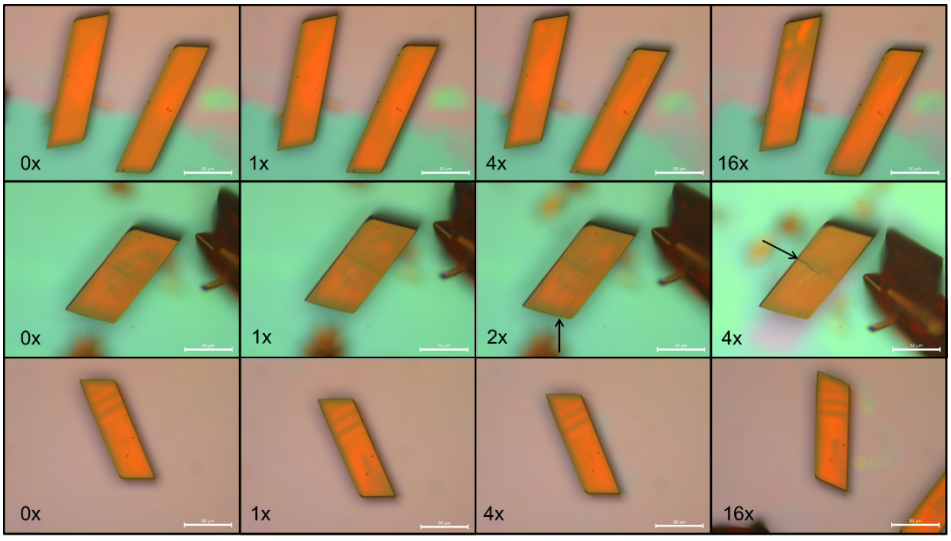

Figure S2.6: SCO events (phase I to phase III) were induced in crystals of compound **1** on silicon wafer by repeatedly cooling to 77 K by immersing them in liquid nitrogen, then heating back to 293 K. Crystals had good resistance against defect formation during multiple spin crossover cycles (top, bottom), but formation of defects could trigger crack formation in the crystal, indicated by the arrows (middle). Scale bar = 50 μm.

Resistance measurements with varying spacer thickness

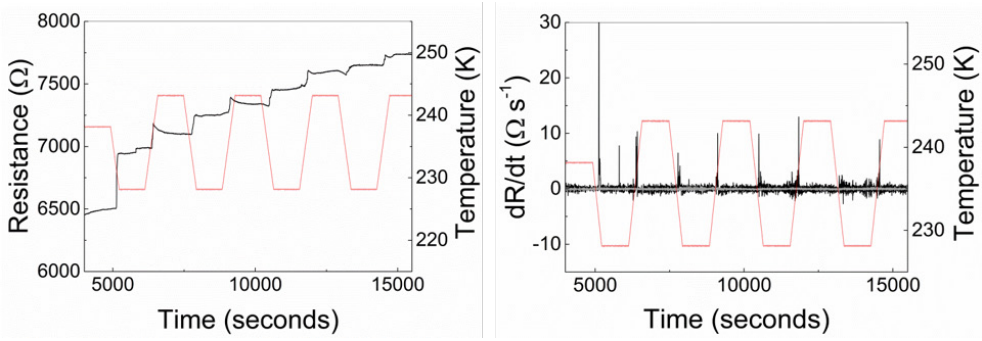

Figure S2.7: *R* and *T vs.* time and *dR/dt* and *T vs.* time for a device with 0 μm spacer.

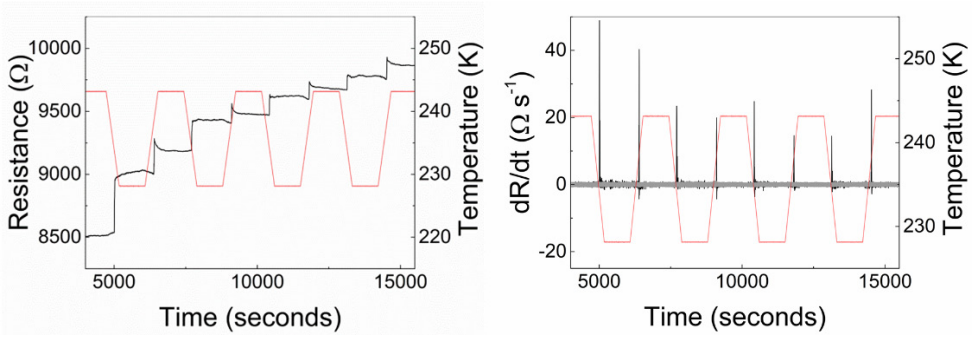

Figure S2.8: *R* and *T vs.* time and *dR/dt* and *T vs.* time for a device with 0.1 μm spacer.

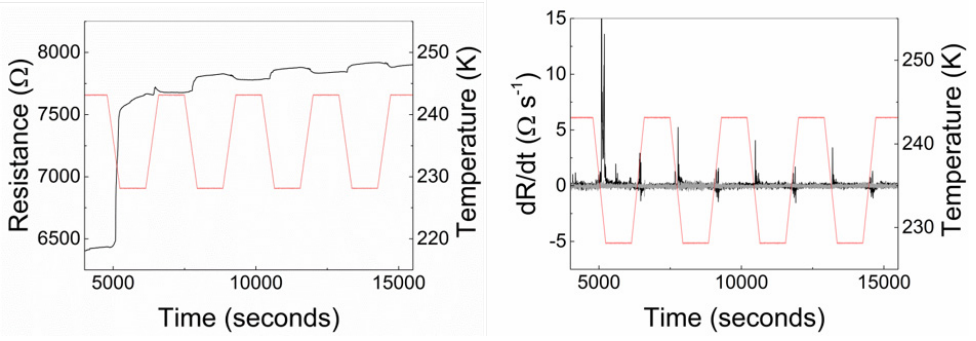

Figure S2.9: *R* and *T vs.* time and *dR/dt* and *T vs.* time for a device with 0.3 μm spacer.

I/V characterization of GFET before and after temperature cycling

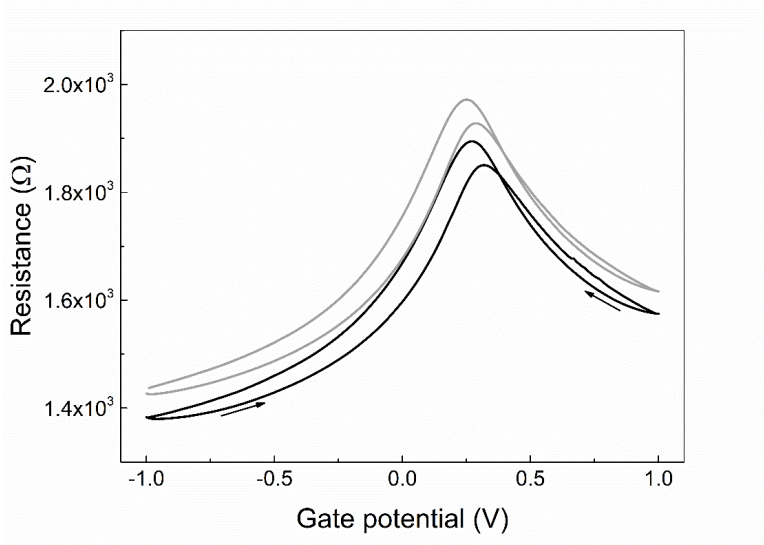

Figure S2.10: Resistance *vs.* gate potential for a device with a 0.5 μm spacer, at 293 K, before (black) and after (grey) a temperature cycle; from 293 to 213 K and back, steps of 10 K outside SCO region and 5 K in SCO region, where the SCO region is from 243 to 223 K. Gate potential was varied at 0.01 Vs^{-1}.

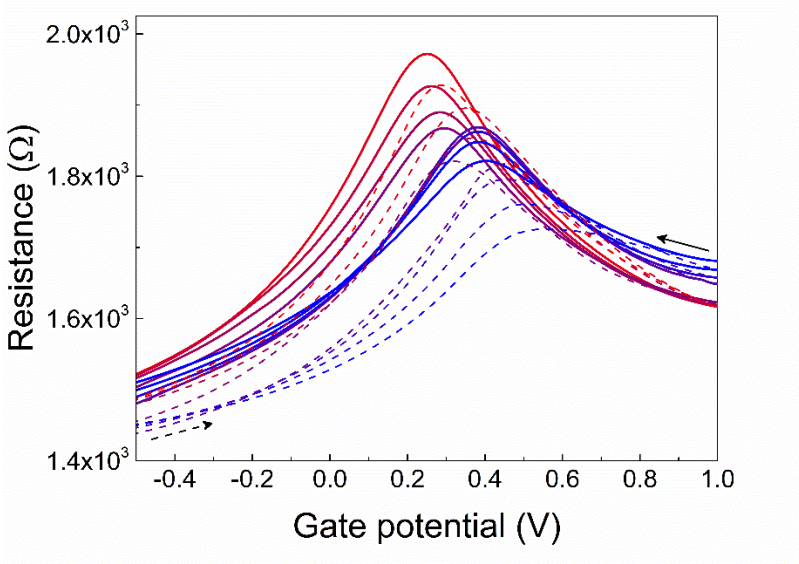

Figure S2.11: Resistance *vs.* gate potential for forward and backward sweeps at different temperatures (recorded during heating mode, from 223 K to 293 K, indicated by blue and red, respectively). Solid lines represent gate sweeps from +1.0 V to -1.0 V, dashed lines represent the opposite direction, -1.0 V to +1.0 V.

Supplementary Text

Phase-dependent electrostatic potential of Fe(bapbpy)(NCS)$_2$

The long-range electrostatic potential induced by the SCO crystal has been computed from the data presented in Table S2.2. Given the micrometer-scale dimensions of the grown crystal consisting of roughly 10^{15}-10^{17} atoms, a direct numerical approach to the induced potential comes with high computational costs. To avoid this computational bottleneck, the crystal has been modeled according to Figure S2.12 by a set of parallel charged sheets stacked on top of one another, each of which yields an electric potential of

$$\phi_i(y) = -\frac{\sigma_i}{2\epsilon_r\epsilon_0}y + \phi_0, \qquad \text{(S1)}$$

at the normal distance $y \gg \max(a_x, c_z)$, where a_x and c_z are the in-plane lattice constants. In equation (S1), $\sigma_i = c_i/(a_x c_z)$ is the charge density per unit area which depends on the net atomic charge c_i (see Table S2.2), ϵ_r is the relative permittivity of the surrounding substance, and ϕ_0 is the constant reference potential. The overall potential ϕ at the place of graphene is thus given by superimposing partial contributions from all charged planes as

$$\phi = -\sum_i \left[\frac{\sigma_i}{2\epsilon_0}\left(\frac{h}{\epsilon_r^{PMMA}} + \frac{\delta_i}{\epsilon_r^{SCO}}\right) + \phi_0\right]. \qquad \text{(S2)}$$

Here, h is the thickness of the PMMA spacer and $h + \delta_i$ specifies the distance between the ith charged plane and the graphene sheet. In view of the fact that the SCO complex is electronically neutral ($\sum_i \sigma_i = 0$), the first contribution in equation (S2) vanishes. Therefore, the potential shift arising from a phase transition, for instance IP → HS (phase II to phase I), can be calculated from

$$\phi^{HS} - \phi^{IP} = -\frac{1}{2\epsilon_r^{SCO}\epsilon_0}\sum_i\left(\sigma_i^{HS}\delta_i^{HS} - \sigma_i^{IP}\delta_i^{IP}\right). \qquad \text{(S3)}$$

For simplicity, in deriving equation (S3), we have omitted the dependence of the dielectric parameter ϵ_r^{SCO} on variations of the electronic state during IP ⇌ HS transitions. We note, however, that the hysteretic deviations of ϵ_r^{SCO}, which have been observed experimentally for similar SCO compounds,[3] are sufficiently superficial to have no severe consequences for the induced potential drop.

To further lift the computational burden, the sum over i in equation (S3) can be split according to the periodicity of the crystal along the stacking direction y. Assuming that the crystal surface resembles an array of N iterative slabs whose thickness is Nb_y, where b_y is the lattice constant along the stacking direction, the first sum in equation (S3) yields

$$\sum_i \sigma_i^{HS}\delta_i^{HS} = \sum_{n=0}^{N-1}\sum_{j=1}^{M}\sigma_j^{HS}\left(\delta_j^{HS} + nb_y\right) = N\sum_{j=1}^{M}\sigma_j^{HS}\delta_j^{HS} + \sum_{n=0}^{N-1} nb_y \sum_{j=1}^{M}\sigma_j^{HS}, \qquad \text{(S4)}$$

where j enumerates the charged sheets per slab. Given the charge neutrality of each slab, *i.e.*, $\sum_{j=1}^{M}\sigma_j^{HS} = 0$, we directly obtain from equations (3) and (4) that

$$\phi^{HS} - \phi^{IP} = -\frac{N}{2\epsilon_r^{CO}\epsilon_0}\sum_{j=1}^{M}\left(\sigma_j^{HS}\delta_j^{HS} - \sigma_j^{IP}\delta_j^{IP}\right). \qquad \text{(S5)}$$

The potential shift $\Delta\phi = |\phi^{HS} - \phi^{IP}|$ is presented in Table S2.1 for different thicknesses Nb_y of the SCO crystal. It is worth mentioning that the theoretical model above holds true as long as the thickness h of the PMMA spacer is small compared to the length and width of the crystal surface. In this case, h has no influence on the remote detection of SCO events in the crystal, which is fully consistent with our experimental observations.

Table S2.1: Potential shift $\boldsymbol{\Delta\phi = |\phi^{HS} - \phi^{IP}|}$, in volts, for different thicknesses of the SCO crystal. The dielectric constant $\boldsymbol{\epsilon_r^{SCO} \approx 4}$. The normal lattice constant at IP and HS phases is $\boldsymbol{b_y}$ = 10.72 and 10.97 Å, respectively.

N ($\times 10^4$)	Thickness at IP phase [μm]	$\Delta\phi$ [V]
2	21.4	0.017
4	42.9	0.033
6	64.3	0.050
8	85.8	0.067
10	107.2	0.083

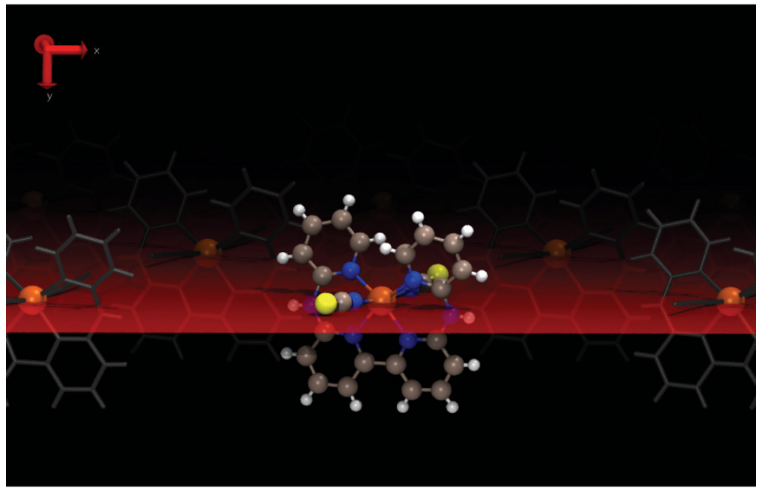

Figure S2.12: Side view of the uppermost surface layer of crystalline [Fe(bapbpy)(NCS)$_2$] which is extended parallel to the (x,z) plane. The flat plane shown in red contains Fe atoms which, in micrometer scale, make an extended charged sheet with a uniform charge density. Considering a similar scenario for other atoms, the SCO crystal can be modeled by a set of charged sheets stacked parallel to one another. The charge density of each sheet is proportional to the net charge allocated to its individual atoms.

Charge transport in graphene

It has previously been demonstrated by comparing between theory and experiment that the scattering of graphene's mobile carriers by long-range interactions with charged impurities yields a linear conductivity at high carrier densities.[4, 5] Charged impurities, on the other hand, create inhomogeneous potential fluctuations and charge puddles,[6] giving rise to a residual carrier density n^* independent of the applied gate voltage. The presence of n^* in our experiments has been witnessed by a nonzero conductivity measured at the Dirac point, which is much larger than if the conductivity was created by temperature. To address the problem of electronic transport under the influence of charged impurities we employ the semiclassical Boltzmann transport theory,[5-9] according to which the electrical conductivity is given by[8]

$$\sigma = \frac{e^2}{2}\int v_k^2\, D(E)\, \tau(E)\left(-\frac{\partial f}{\partial E}\right) dE. \qquad \text{(S6)}$$

In equation (S6), $\vec{v}_{\boldsymbol{k}} = \left(\frac{1}{\hbar}\right)\vec{\nabla}_{\boldsymbol{k}}E$ corresponds to the group velocity of electrons, $D(E)$ is the density of states per unit area, f the Fermi function, and τ denotes the relaxation time. Assuming that the process of scattering is predominantly elastic, the value of τ for a linear energy dispersion relation $E = \pm\hbar v_F|\boldsymbol{k}|$ (v_F is the Fermi velocity) can be obtained from[9]

$$\frac{1}{\tau(E)} = \frac{n_i}{8\hbar}D(E)\int \left|V_q\right|^2 (1 - cos^2\theta)\, d\theta. \qquad \text{(S7)}$$

Here, n_i is the impurity concentration, V_q is the electrostatic potential created by charged impurities in Fourier space, and $q = 2E\sin(\theta/2)/(\hbar v_F)$ and θ specify the scattering wave vector $qe^{i\theta}$ in polar coordinates. Owing to the fact that V_q is screened by graphene's two-dimensional electron system, we obtain[5, 6]

$$V_q = \frac{e^2}{2\kappa\varepsilon_0\varepsilon(q,T)}\, e^{-qd}, \qquad \text{(S8)}$$

where $\kappa \approx 3.8$ is the background dielectric constant, d corresponds to the normal distance of graphene from charged impurities, and ε is the static dielectric function. The procedure of calculating $\varepsilon(q,T)$, within the random phase approximation (RPA), has been detailed in Ref. [10]. Nevertheless, for temperatures much less than the Fermi temperature, *i.e.*, $T \ll T_F$, it is possible to describe ε using the following analytical expression[10]

$$\varepsilon(q, T \ll T_F) \approx \frac{\widetilde{\kappa}}{k} + \frac{g_{sv}r_s k_F}{q}\begin{cases} 1 - \frac{\pi q}{8k_F} & q \le 2k_F, \\ 1 - \frac{1}{2}\sqrt{1 - \left(\frac{2k_F}{q}\right)^2} - \frac{q}{4k_F}sin^{-1}\frac{2k_F}{q} & q > 2k_F, \end{cases} \qquad \text{(S9)}$$

where $g_{sv} = 4$ accounts for the spin and valley degrees of freedom of electrons in graphene, and $\tilde{\kappa} = \kappa\left(1 + \frac{g_{sv}\pi r_s}{8}\right)$ is the effective dielectric constant with $r_s = e^2/(4\pi\epsilon_0\kappa\hbar v_F)$ being the fine structure.

In order to compare the measured transport components with theory, the conductivity σ (equation S6) has to be computed as a function of the top gate voltage V_g. To do so, it is first necessary to obtain the V_g-induced doping concentration (n_g) according to[11]

$$V_g = \frac{\hbar v_F \sqrt{\pi n_g}}{e} + \frac{e n_g}{C_g}, \qquad \text{(S10)}$$

where C_g is the geometric capacitance due to formation of a nanometer-thick Debye layer at graphene/PMMA-ionic liquid interface. Subsequently, the effective carrier density characterizing the electrical conductivity is given, as an approximation, by $n = |n_g| + |n^*|$.[12] As the last step, we must evaluate the residual carrier density n^*. For doing this, we employed a self-consistent theory,[6] according to which n^* is explicitly a function of the impurity density n_i, *i.e.*,

$$n^* = 2\, r_s\, n_i\, C_0^{RPA}\left(r_s, 4d\sqrt{\pi n^*}\right), \qquad \text{(S11)}$$

where C_0^{RPA} is the correlation function obtained from the random phase approximation.

Phonon-limited resistivity

Although the dominant contribution to the resistivity of our graphene sample originates from the electrostatic scattering by charged impurities, the effect of electron-phonon interaction has also been incorporated into our transport calculations as a minor correction. To this end, we have used the Boltzmann transport equation. By simplifying this equation using variational methods, the phonon-limited resistivity is given by[13]

$$\rho_{e-ph} = \frac{3\sqrt{3}\,\pi a^2}{e^2 n_\uparrow v^2} \int_0^\infty \frac{\frac{\hbar\omega}{2k_BT}}{\sinh^2\left(\frac{\hbar\omega}{2k_BT}\right)}\, \alpha_{tr}^2 F(\omega)\, d\omega, \qquad \text{(S12)}$$

where $a \approx 1.4076$ Å is the C-C bond length, v the velocity averaged over the Fermi surface, and $n_\uparrow$ is the density of states per unit cell per spin at E_F. In equation (S12), the transport Eliashberg function $\alpha_{tr}^2 F(\omega)$ is determined by the electron-phonon coupling as follows

$$\alpha_{tr}^2 F(\omega) = \frac{1}{n_\uparrow A_{bz}^2} \sum_{m'mv} \iint d\boldsymbol{p}\, d\boldsymbol{q}\, \left|g^v_{m',m}(\boldsymbol{p},\boldsymbol{q})\right|^2 \times \left(1 - \frac{\boldsymbol{v}_{p+q,m'} \cdot \boldsymbol{v}_{p,m}}{|\boldsymbol{v}_{p,m}|^2}\right)$$
$$\times\, \delta\left(\epsilon_{\boldsymbol{p}+\boldsymbol{q},m'} - E_F\right)\delta\left(\epsilon_{\boldsymbol{p},m} - E_F\right)\, \delta\left(\hbar\omega^v_{\boldsymbol{q}} - \hbar\omega\right). \qquad \text{(S13)}$$

Here, $A_{bz} = 8\sqrt{3}\pi^2/9a^2$ is the area of the first Brillouin zone of graphene, $|\boldsymbol{p}+\boldsymbol{q}, m'\rangle$ and $|\boldsymbol{p}, m\rangle$ correspond to the final and initial scattering states, respectively, and $\omega^v_{\boldsymbol{q}}$ denotes the angular frequency of the v-th phonon mode for wave vector $\boldsymbol{q}$. The elements of the electron-phonon interaction matrix, *i.e.*, $g^v_{m',m}(\boldsymbol{p},\boldsymbol{q})$, have already been modeled by Park *et al.*[13] using the local density approximation (LDA) method (see Table 1 in Ref. 13).

By evaluating equation (S12) for the experimental temperatures T = 238 and 243 K we concluded that the contribution of ρ_{e-ph} to the overall resistivity is roughly two orders of magnitude less than that of charged impurities.

Charge distribution in the HS and LS molecules

Complete active space self-consistent field (CASSCF) calculations were performed upon the isolated basic units of the [Fe(bapbpy)$(NCS)_2$] complex. This methodology, working with the exact Hamiltonian, is known to provide satisfactory descriptions of electronic structures, which is a major concern in our approach. A limited number of electrons distributed over a set of valence molecular orbitals defined the complete active space (CAS). As reported in literature,[14] the standard CAS consists of the 3d orbitals with mainly Fe character, extended with a set of virtual orbitals of the same symmetry (so-called 3d' orbitals), and two occupied "e_g-like" symmetry orbitals with mainly ligand character. Thus, a CAS[10,12] including ten electrons in twelve active orbitals was used in the calculations. This extended active space accounts for the important charge fluctuations accompanying the S=0 → S=2 spin change. Net charges were estimated from the LoProp tool, based on the one-electron density. The values we used were slightly different from the ones given in a previous inspection,[15] since charges were then condensed onto the iron and the surrounding nitrogen atoms.

All our calculations were performed with the Molcas8.0 program,[16] including atomic natural orbitals (ANO-RCC) as basis sets.[17] As stated previously,[14] finely balanced basis sets are necessary to properly describe the energetics of SCO phenomenon. Thus, a [7s6p5d3f2g1h] contraction was used for Fe, whereas the contractions [3s2p1d], [4s3p1d], [4s3p1d], [3s3p1d], and [1s] were used for C, N, O, S, and H, respectively.

Table S2.2: Calculated geometry and total charge for individual atoms and the dipole moment for the complete molecule in the HS and LS state. NB: the origin of the operator for the dipole moments is the Fe atom.

	High spin				**Low spin**			
Atom	x	y	z	Net Charge [Debye]	x	y	z	Net Charge [Debye]
Fe1	0.0000	0.0000	0.0000	1.3900	0.0000	0.0000	0.0000	1.0685
S2	-2.9643	0.5322	-3.8675	-0.4259	-2.8011	-0.2033	-3.8093	-0.4450
S3	2.9643	0.5322	3.8675	-0.4259	2.8671	0.5129	3.7471	-0.4450
N4	-1.2900	1.1720	1.2514	-0.3750	-1.2456	1.1420	1.0319	-0.3234
N5	-3.0302	-0.4078	1.3663	-0.3029	-2.9267	-0.5039	1.1464	-0.2975
N6	-1.1862	-1.6668	0.6103	-0.3886	-0.9265	-1.6088	0.5700	-0.3138
N7	-1.4500	0.2307	-1.5680	-0.5773	-1.1918	-0.0882	-1.5191	-0.4911
N8	1.2900	1.1720	-1.2514	-0.3788	1.3103	-1.2826	-0.6445	-0.3139
N9	3.0302	-0.4078	-1.3663	-0.3096	2.9075	0.3363	-1.2633	-0.2961
N10	1.1862	-1.6668	-0.6103	-0.3301	0.8705	1.4962	-0.9758	-0.3226
N11	1.4500	0.2307	1.5680	-0.5779	1.2006	0.1779	1.5154	-0.4965
C12	-0.8731	2.4176	1.5353	0.0772	-0.8267	2.3646	1.4608	0.0765
C13	-1.6629	3.3813	2.0803	-0.1829	-1.6213	3.2563	2.1113	-0.1781
C14	-2.9704	3.0556	2.3778	-0.0201	-2.9429	2.9096	2.3725	-0.0212
C15	-3.4080	1.7920	2.1427	-0.2064	-3.3708	1.6544	2.0339	-0.2003
C16	-2.5423	0.8598	1.5790	0.3091	-2.4789	0.7743	1.3969	0.3027
C17	-2.4447	-1.6085	1.0545	0.3214	-2.2169	-1.6616	0.9368	0.3071
C18	-3.2346	-2.7522	1.2028	-0.2006	-2.8898	-2.8838	1.0804	-0.1892
C19	-2.7140	-3.9532	0.8726	-0.0192	-2.2245	-4.0506	0.8255	-0.0257
C20	-1.4223	-4.0290	0.3942	-0.1906	-0.9065	-4.0085	0.3956	-0.1705
C21	-0.6898	-2.8772	0.2695	0.1760	-0.3012	-2.7726	0.2512	0.1672
C22	-2.0953	0.3704	-2.5032	0.1281	-1.8753	-0.1297	-2.4467	0.1104
C23	0.6898	-2.8772	-0.2695	0.1443	1.0302	-2.5797	-0.3321	0.1670
C24	1.4223	-4.0290	-0.3942	-0.1499	1.9402	-3.5970	-0.5389	-0.1694
C25	2.7140	-3.9532	-0.8726	-0.0462	3.1869	-3.2810	-1.0626	-0.0263
C26	3.2346	-2.7522	-1.2028	-0.1762	3.4997	-1.9709	-1.3264	-0.1883
C27	2.4447	-1.6085	-1.0545	0.2885	2.5384	-0.9779	-1.0793	0.3067
C28	2.5423	0.8598	-1.5790	0.3110	2.1425	1.4721	-1.3974	0.3046
C29	3.4080	1.7920	-2.1427	-0.2079	2.7562	2.5772	-2.0048	-0.2023
C30	2.9704	3.0556	-2.3778	-0.0199	2.0049	3.6879	-2.2736	-0.0213
C31	1.6629	3.3813	-2.0803	-0.1851	0.6538	3.6804	-1.9578	-0.1810
C32	0.8731	2.4176	-1.5353	0.0772	0.1432	2.5797	-1.3264	0.0788
C33	2.0953	0.3704	2.5032	0.1289	1.9060	0.3323	2.4207	0.1102
H34	0.0117	2.6344	1.3475	0.1388	0.0766	2.6095	1.2947	0.1429
H35	-1.3321	4.2336	2.2480	0.1301	-1.2804	4.1004	2.3826	0.1277
H36	-3.5444	3.6928	2.7356	0.1335	-3.5372	3.5314	2.7782	0.1302
H37	-4.2809	1.5518	2.3569	0.1245	-4.2602	1.3809	2.2267	0.1227
H38	-4.1043	-2.6875	1.5235	0.1274	-3.7991	-2.9005	1.3530	0.1246
H39	-3.2246	-4.7254	0.9676	0.1354	-2.6638	-4.8855	0.9396	0.1324
H40	-1.0528	-4.8504	0.1596	0.1263	-0.4313	-4.8095	0.2067	0.1263
H41	1.0528	-4.8504	-0.1596	0.1276	1.7180	-4.4958	-0.3284	0.1261
H42	3.2246	-4.7254	-0.9676	0.1342	3.8187	-3.9679	-1.2376	0.1326
H43	4.1043	-2.6875	-1.5236	0.1288	4.3536	-1.7402	-1.6700	0.1247
H44	4.2809	1.5518	-2.3569	0.1242	3.6799	2.5559	-2.2254	0.1224
H45	3.5444	3.6928	-2.7356	0.1333	2.4013	4.4537	-2.6705	0.1299
H46	1.3321	4.2336	-2.2480	0.1298	0.0974	4.4199	-2.1734	0.1275
H47	-0.0117	2.6344	-1.3475	0.1384	-0.7839	2.5759	-1.1222	0.1410
H48	-3.8284	-0.4938	1.6147	0.2571	-3.7546	-0.6650	1.3352	0.2548
H49	3.8284	-0.4938	-1.6147	0.2559	3.7296	0.4022	-1.5432	0.2530
Dipole moment	-0.2011	-1.1705	-0.0759	Total (Debye) **1.1901**	-0.0126	-3.8956	0.0342	Total (Debye) **3.8958**

References

[1] S. Bonnet, M. A. Siegler, J. S. Costa, G. Molnar, A. Bousseksou, A. L. Spek, P. Gamez, J. Reedijk, *Chem. Commun.* **2008**, *0*, 5619.
[2] S. Zheng, M. A. Siegler, O. Roubeau, S. Bonnet, *Inorg. Chem.* **2014**, *53*, 13162.
[3] T. Guillon, S. Bonhommeau, J. S. Costa, A. Zwick, J.-F. Létard, P. Demont, G. Molnár, A. Bousseksou, *Phys. Status Solidi A* **2006**, *203*, 2974; A. Bousseksou, G. Molnár, P. Demont, J. Menegotto, *J. Mater. Chem.* **2003**, *13*, 2069.
[4] J. H. Chen, C. Jang, S. Adam, M. S. Fuhrer, E. D. Williams, M. Ishigami, *Nat. Phys.* **2008**, *4*, 377.
[5] E. H. Hwang, S. Adam, S. D. Sarma, *Phys. Rev. Lett.* **2007**, *98*, 186806.
[6] S. Adam, E. H. Hwang, V. M. Galitski, S. Das Sarma, *Proc. Natl. Acad. Sci.* **2007**, *104*, 18392.
[7] T. Ando, *J. Phys. Soc. Jpn.* **2006**, *75*, 074716.
[8] S. Das Sarma, S. Adam, E. H. Hwang, E. Rossi, *Rev. Mod. Phys.* **2011**, *83*, 407.
[9] T. Stauber, N. M. R. Peres, F. Guinea, *Phys. Rev. B* **2007**, *76*, 205423.
[10] E. H. Hwang, S. Das Sarma, *Phys. Rev. B* **2007**, *75*, 205418.
[11] A. Das, S. Pisana, B. Chakraborty, S. Piscanec, S. K. Saha, U. V. Waghmare, K. S. Novoselov, H. R. Krishnamurthy, A. K. Geim, A. C. Ferrari, A. K. Sood, *Nat. Nanotechnol.* **2008**, *3*, 210.
[12] J. Xia, F. Chen, J. Li, N. Tao, *Nat. Nanotechnol.* **2009**, *4*, 505; S. Samaddar, I. Yudhistira, S. Adam, H. Courtois, C. B. Winkelmann, *Phys. Rev. Lett.* **2016**, *116*, 126804.
[13] C.-H. Park, N. Bonini, T. Sohier, G. Samsonidze, B. Kozinsky, M. Calandra, F. Mauri, N. Marzari, *Nano Lett.* **2014**, *14*, 1113.
[14] M. Kepenekian, V. Robert, B. Le Guennic, C. De Graaf, *J. Comput. Chem.* **2009**, *30*, 2327.
[15] M. Kepenekian, J. S. Costa, B. Le Guennic, P. Maldivi, S. Bonnet, J. Reedijk, P. Gamez, V. Robert, *Inorg. Chem.* **2010**, *49*, 11057.
[16] F. Aquilante, J. Autschbach, R. K. Carlson, L. F. Chibotaru, M. G. Delcey, L. De Vico, I. Fdez. Galván, N. Ferré, L. M. Frutos, L. Gagliardi, M. Garavelli, A. Giussani, C. E. Hoyer, G. Li Manni, H. Lischka, D. Ma, P. Å. Malmqvist, T. Müller, A. Nenov, M. Olivucci, T. B. Pedersen, D. Peng, F. Plasser, B. Pritchard, M. Reiher, I. Rivalta, I. Schapiro, J. Segarra-Martí, M. Stenrup, D. G. Truhlar, L. Ungur, A. Valentini, S. Vancoillie, V. Veryazov, V. P. Vysotskiy, O. Weingart, F. Zapata, R. Lindh, *J. Comput. Chem.* **2015**, *37*, 506.
[17] B. O. Roos, R. Lindh, P.-Å. Malmqvist, V. Veryazov, P.-O. Widmark, *J. Phys. Chem. A* **2004**, *108*, 2851.

Appendix

Chapter 3

Materials and Methods

Bapbpy was synthesized using a previously reported protocol.[1] Single crystals of [Fe(bapbpy)$(NCS)_2$] were prepared using an adapted liquid-liquid diffusion method developed in our group.[2] Shortly, a DMF-resistant single-use cuvette (BRAND® UV microcuvette) was placed in a glass snap-cap vial (VWR, 10 ml, 22x50 mm). A wafer (typically 15x8 mm Prime grade, 285 nm SiO_2, single-side polished, Siegert Wafer GmbH) was placed vertically in the cuvette. The cuvette was put under N_2 and closed with the snap-cap, and a solution of [Fe$(SCN)_2$] in methanol (0.1 M, 0.035 ml) was added with a solution of bapbpy in DMF (15 mM, 0.22 ml, filtrated before use). Both solutions were degassed by the freeze-pump-thaw method beforehand; solutions were added with a needle-fitted gas-tight syringe through the snap-cap to disturb the N_2 atmosphere as little as possible. The solutions were mixed by shaking. Next, 2.0 ml of methanol (degassed by N_2 bubbling, with ~5 mg ascorbic acid) was added in the snap-cap vial for vapor diffusion into the solution in the cuvette. After addition of all solutions, the punctured caps were replaced with intact ones carefully, to not disturb the atmosphere in the vial. For thin film formation, the wafer was left one or multiple days in solution before extracting, rinsing with methanol and blow-drying the wafer.

Monolayer graphene was home-grown on Cu foil (Alfa Aesar, 0.025 mm, Puratronic©, 99.999% metals basis) using a hot-wall tube CVD oven. Graphene on copper was spin-coated with PMMA (6% in anisole, Allresist GmbH., AR-P 662.06; 4000 rpm for 60 s, heated at 85°C for 10 minutes, then back-etched in oxygen plasma (0.30 mbar, 100 W, 2 minutes) and transferred on a cleaned wafer (sonication in acetone for 5 min, then rinsed with acetone, MilliQ and isopropanol, then treated with O_2 plasma (0.30 mbar, 100 W, 2 minutes), optionally with Au electrodes deposited beforehand. Au electrodes were fabricated on clean wafers by metal sputtering; first, a wafer was masked with aluminum foil with cutouts where the electrodes will be deposited. To assure adhesion of the gold to the wafer, a layer of chromium (5 nm) was deposited, after which 75 nm of gold was deposited. Wafers with Au electrodes were cleaned in the same way as bare wafers (see above) prior to graphene transfer.

Graphene was transferred using PMMA-assisted the transfer method by etching copper with an ammonium persulfate solution (0.2 M in MilliQ) and rinsing the PMMA-graphene film by transferring it in three MilliQ baths consecutively, after which this film was transferred on the wafer by fishing the floating film from below. Next, water was allowed to gently evaporate at 45°C; when water was evaporated, the coated wafer was heated at 150°C for 15 minutes. After successful transfer, the PMMA layer was removed by immersing the wafer in acetone for 10 minutes, then rinsing gently with acetone, ethanol and isopropyl alcohol, and blowing the wafer dry with pressurized air. In the case of wafers with Au electrodes, the electrodes were connected using electrically conductive silver epoxy (Gentec, EPOTEK EJ2189-LV) to copper wires. The wafer was heated to 150°C for 15 minutes to cure the conductive epoxy.

Graphene on silicon wafer was patterned with μ-contact printing. A PDMS stamp with the pattern was coated with a PMMA solution (6 wt% in anisole) using spin coating (15 seconds, 4000 rpm, acceleration 500 rpm/s), after which the stamp was pressed on a wafer on which graphene was transferred (PMMA-assisted) and exposed beforehand. After successful printing of the polymeric mask, excess graphene was removed through standard oxygen plasma cleaning. Finally, the polymeric mask was removed by immersion in acetone for 10 minutes and the wafer with exposed

patterned graphene was rinsed with acetone, ethanol and isopropyl alcohol and blown dry with pressurized air.

Oxygen plasma was generated using a capacitively coupled plasma system with radio-frequency of 40 kHz and 200 W power from Diener electronic (Femto), employed at room temperature. Spin coating was using with a POLOS SPIN150i tabletop spin coater. Optical images were obtained using a Leica DM2700 M Brightfield microscope fitted with Leica MC120 HD camera. AFM images were recorded on a JPK Nanowizard Ultra. Raman spectra were recorded on a Witec Alpha500 R Raman spectrometer using a 532 nm laser at low power (0.23 mW). EDX mapping was performed on an Apreo Scanning Electron Microscope (SEM). XPS spectra were recorded on a ThermoScientific K-Alpha spectrometer fitted with a monochromatic X-ray source. XRD spectra were recorded with a Bruker D8 Advance diffractometer using Cu Kα radiation (λ = 1.5406 Å). Magnetic measurements were performed using a Quantum Design MPMS XL SQUID Magnetometer. Electrical characterization of devices was performed using Keithley Sourcemeters, models 2450 and 2400, in combination with Kickstart measuring software. Optical footage of a device inside the chamber was recorded using the optical camera equipped to the Raman microscope setup. Temperature cycling experiments were performed using a Linkam THMS600E microscope heating/cooling stage equipped on the Raman spectrometer in combination with LINK temperature control software. During temperature cycle experiments, the devices were electrically connected inside the heating/cooling stage. To prevent condensation, the chamber was purged with N_2 (N3.0) at the start each experiment, according to the manufacturer's protocol.

Supplementary Figures

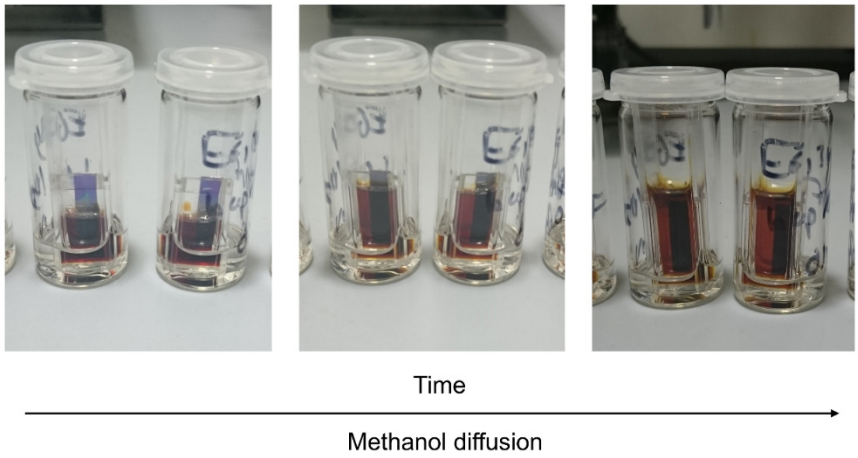

Figure S3.1: Photograph of a typical thin film growing experiment. Methanol diffused from the vial to the cuvette that is inside.

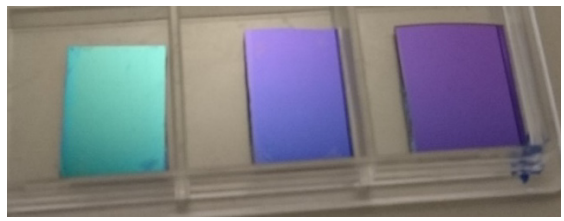

Figure S3.2: Camera images of wafer fully coated with thin film-coated graphene on wafer (left, blue-green, 5 days film growth), wafer fully coated with graphene (center, deep blue) and uncoated wafer (right, purple).

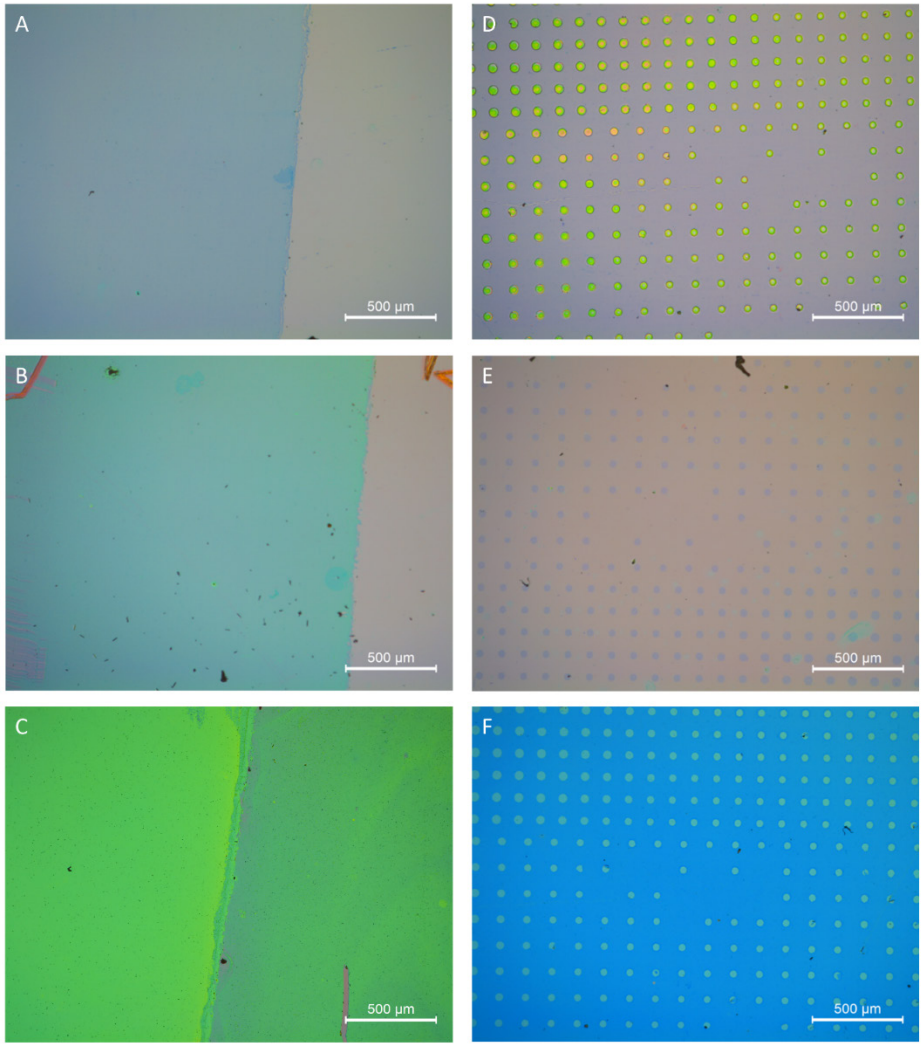

Figure S3.3: Optical microscopy images of 1 day, 2 day and 6 days of film formation (A-C) on graphene, always on the left side of the wafer. The scratch in C) reveals the wafer underneath the thin film, showing the thin film has deposited on the wafer itself as well. D-F) optical microscopy images of patterning and growing films on graphene, showing patterned PMMA mask on graphene (D), exposed graphene after oxygen plasma and removal of the polymer mask (E), and thin film grown on graphene (F, growth time = 6 days).

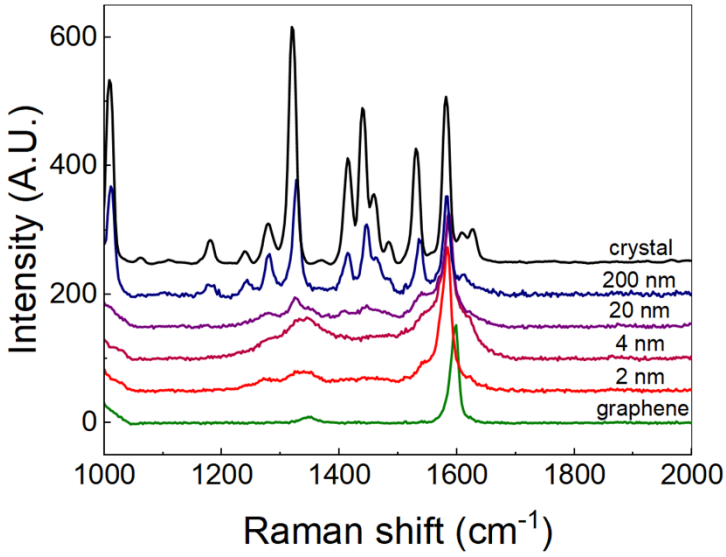

Figure S3.4: Raman spectrum (zoomed) of bare graphene on silicon wafer (green), graphene coated with thin films of [Fe(bapbpy)$(NCS)_2$] with different thicknesses (red to blue), and single crystals of the HS phase of [Fe(bapbpy)$(NCS)_2$] (black) at room temperature.

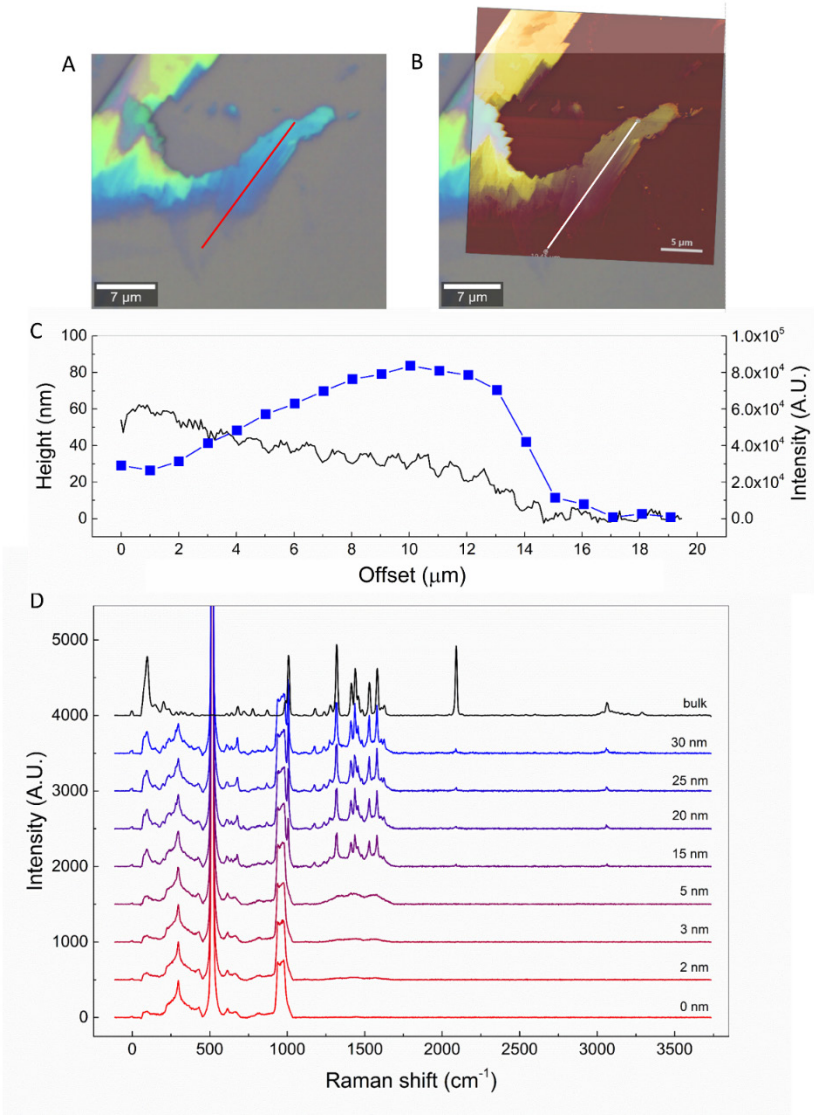

Figure S3.5: Raman spectroscopy of thin residue material from [Fe(bapbpy)(NCS)$_2$] bulk crystal, damaged with sonication. A) Optical image of thin residue from bulk crystal. Red line indicates line across which Raman spectra were recorded. B) Overlay of optical image shown in A and AFM map of the area. C) Height profile across white line in AFM map (black), overlaying the line along which Raman spectra were recorded, and total peak area from Raman spectroscopy in the range of 1200-1700 cm^{-1} (blue squares). Lower Raman signal from 0 to 10 µm offset is due to out-of-focus measurement; focus is regained for 10 to 20 µm offset. D) Raman spectra of the thin residue at different thicknesses (red to blue) and Raman from an intact [Fe(bapbpy)(NCS)$_2$] crystal (black). Peaks at from 0-1000 cm^{-1} at 0 nm are the background peaks from the silicon wafer.

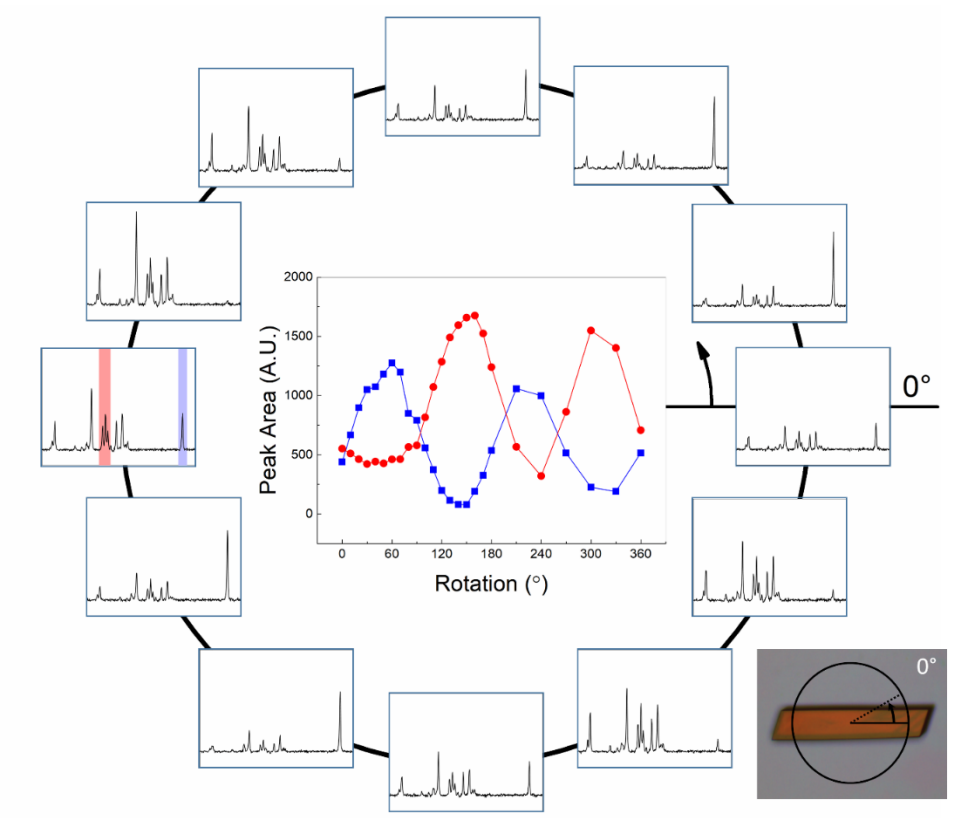

Figure S3.6: Raman spectroscopy of a single crystal of [Fe(bapbpy)(NCS)$_2$] (optical image in the bottom right), rotated anticlockwise in the x,y plane. Individual spectra are displayed on the circle and are scaled equally; their location on the circle indicates the rotation. Red and blue areas at 180° indicate the areas that were integrated to obtain the peak area *vs.* rotation (center), where red corresponds to one of the bapbpy ligand peaks (integrated over 1375-1500 cm^{-1}) and blue corresponds to the thiocyanate peak (integrated over 2050-2150 cm^{-1}).

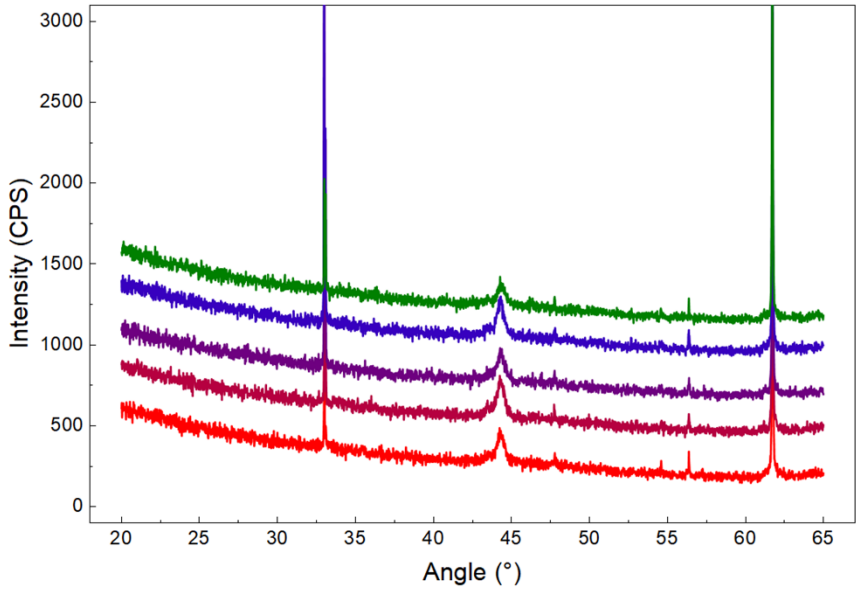

Figure S3.7: XRD spectra of thin films grown on graphene with different growing times on silicon wafer (red to blue: 0 days, 1 day, 2 days, 5 days) and clean silicon wafer (green).

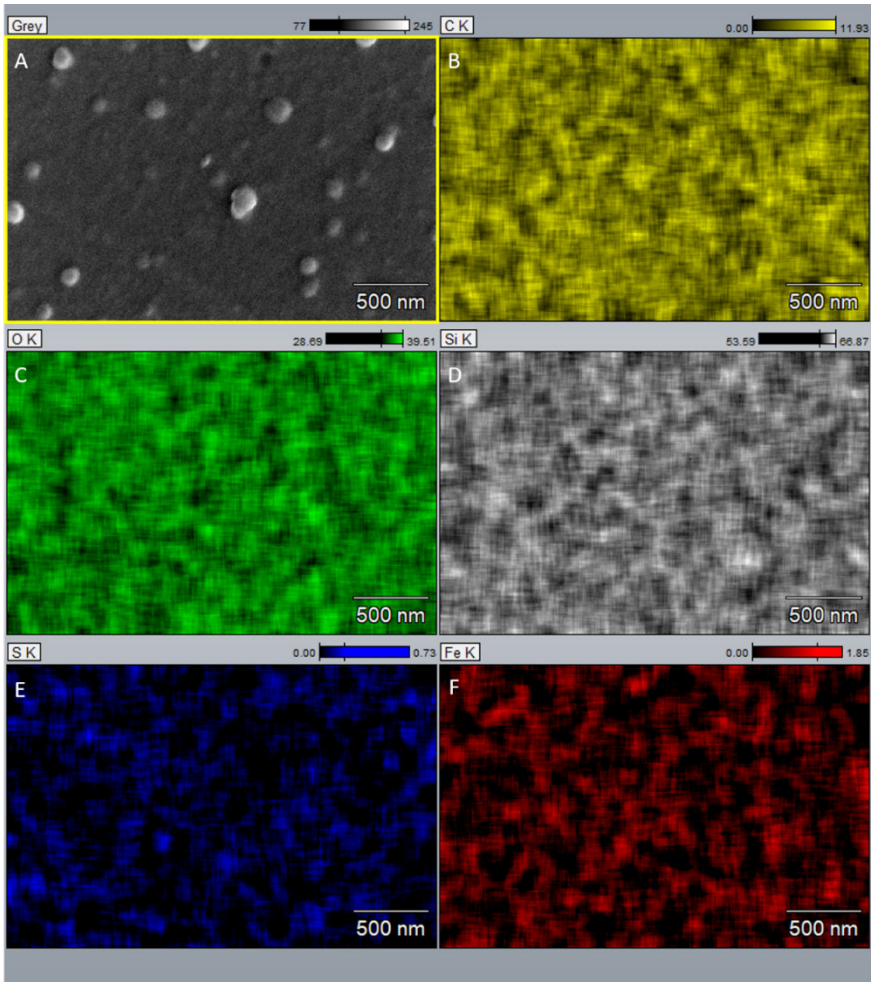

Figure S3.8: EDX analysis of a thin film on graphene. A) SEM image of a thin film on graphene, growth time was 5 days. EDX mapping of the elements carbon (B, yellow), oxygen (C, green), silicon (D, gray), sulfur (E, blue) and iron (F, red).

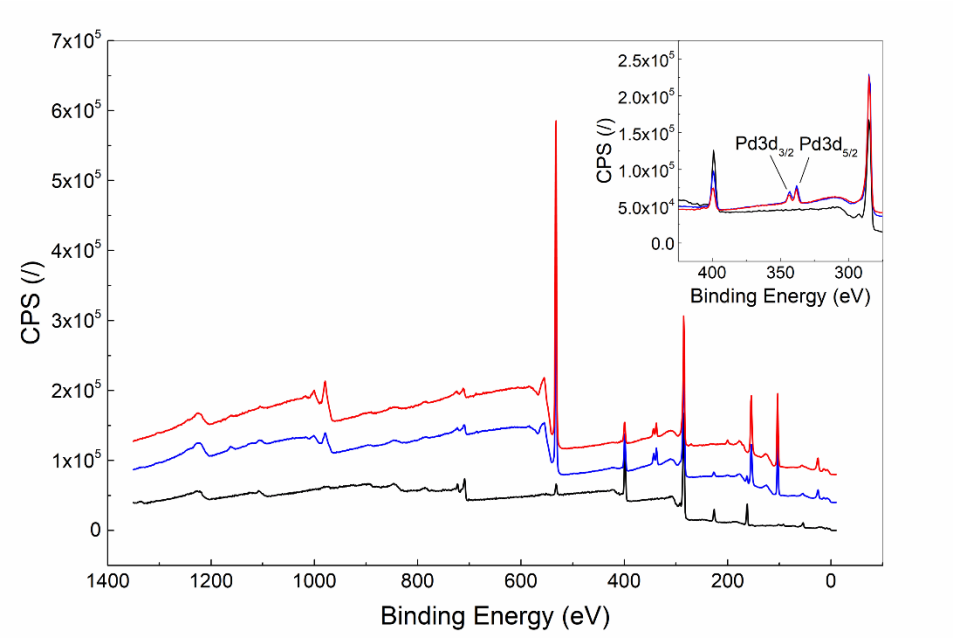

Figure S3.9: XPS spectra of thin film on graphene (growth time 3 days) grown under nitrogen (blue) and under normoxic atmosphere (red), and [Fe(bapbpy)(NCS)$_2$] bulk material which was ground under nitrogen atmosphere (black). Notably, we found that a palladium contamination, likely originating from the ligand synthesis was transferred to the thin films, indicated by a clear doublet in the XPS spectrum of each examined film (338.0 eV and 342.9 eV, see inset).

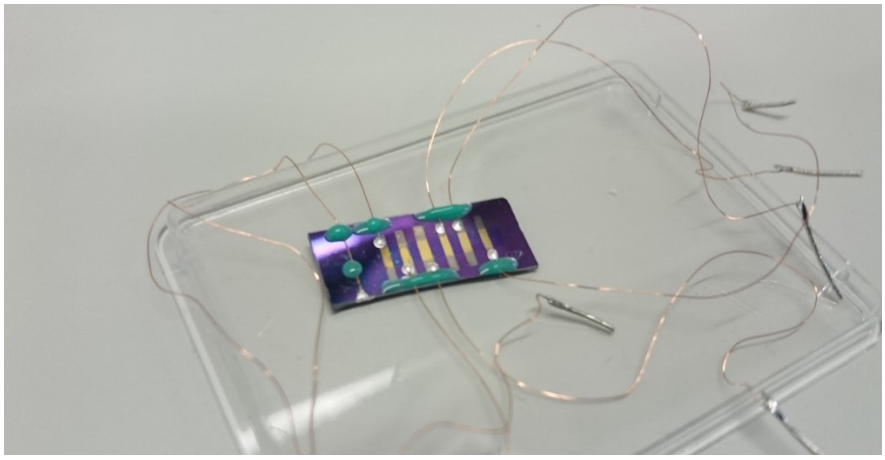

Figure S3.10: Optical image of a GFET coated with a chemically grown thin film, growth time is 2 days.

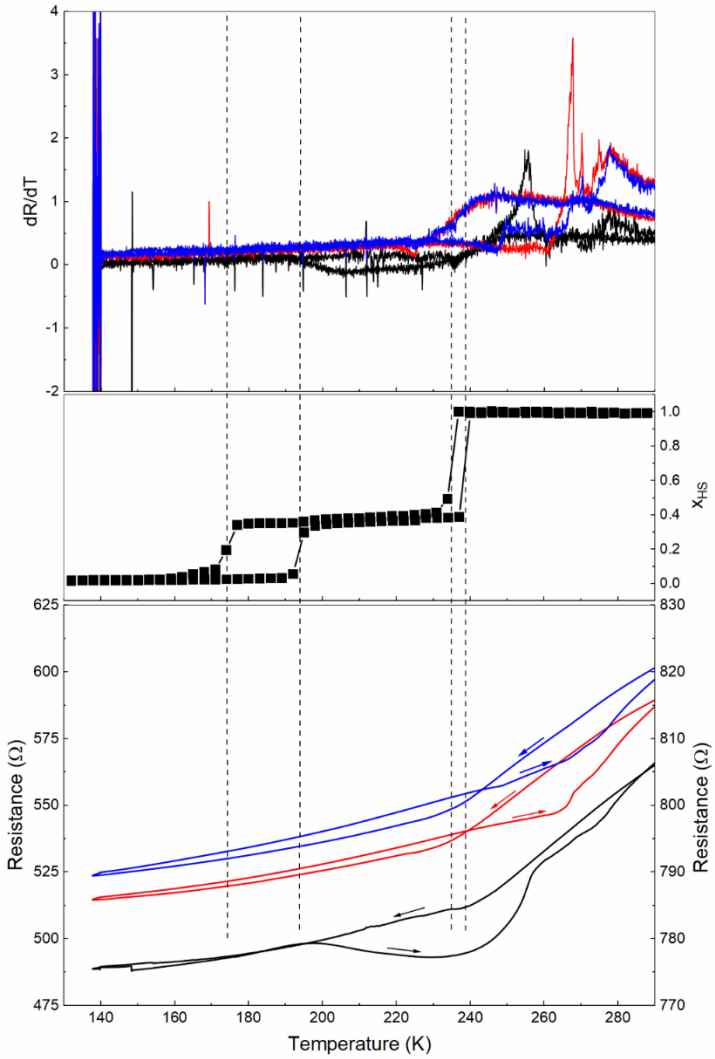

Figure S3.11: *dR/dT* and resistance *vs.* temperature for GFETs coated with a chemically grown thin film, growth time either 0, 1 day or 2 days (black; right axis *R*, red and blue; left axis *R*, respectively), based on [Fe(bapbpy)(NCS)$_2$]. Current I_{AF} was set to 100 μA. Gate voltage was set to 0 V. Temperature was cycled at 2 Kmin^{-1}. Mole fraction of high spin molecules (obtained from $\chi_m T$ measurements using SQUID magnetometry, as was previously reported[1]) in single crystals of [Fe(bapbpy)(NCS)$_2$] is shown above (black squares); spin crossover transition temperatures are indicated by dashed lines.

References and notes

[1] S. Bonnet, M. A. Siegler, J. S. Costa, G. Molnar, A. Bousseksou, A. L. Spek, P. Gamez, J. Reedijk, *Chem. Commun.* **2008**, 0, 5619.

[2] S. Zheng, M. A. Siegler, O. Roubeau, S. Bonnet, *Inorg. Chem*. **2014**, 53, 13162.

Appendix

Chapter 4

Materials and Methods

PMMA solutions were purchased from Allresist GmbH. All chemicals, including a solution of Nafion® 117 (~5% in lower aliphatic alcohols and water, 70160-25ML) and CAB (Mn ~30.000, 419052-250G) powder were obtained from Sigma Aldrich.

Oxygen plasma was generated using a capacitively coupled plasma system with radio-frequency of 40 kHz and 200 W power from Diener electronic (Femto), employed at room temperature. Spin coating was done with a POLOS SPIN150i tabletop spin coater. Electrical characterization of devices was performed using Keithley Sourcemeters model 2450 and 2400 in combination with Kickstart measuring software.

Experimental

PMMA-coated devices (MEAS & REF)

Sensors for manual injection were produced using solely benchtop techniques, without the need of a cleanroom. A silicon wafer of 10 x 20 mm (Prime grade, 285 nm SiO_2 on 0.5 mm Si, single side polished, Siegert Wafer GmbH) was cleaned by sonication in acetone for 5 min, then rinsed with acetone, water and 2-propanol. Next, the wafer was treated with oxygen plasma (0.30 mbar, 100 W, 2 min), after which the wafer was masked with masking tape (Semiconductor Wafer Tape SWT 20+, Nitto Europe N.V.) which had the electrodes shape cut out previously. A mask typically had 6 electrodes (A-F) parallel to each other precut, *i.e.* cutting was not done on the wafer to prevent scratching of the SiO_2 layer at the risk of gate leakage. Electrodes were produced by a chemical silver deposition method using a Tollens' reagent (an aqueous $[Ag(NH_3)_2]^+$ solution). The silvering solutions (A and B) were prepared as follows:

A: To a solution of silver nitrate (0.1 M in water, 25 ml), a potassium hydroxide solution (0.8 M in water, 25 ml) was added, upon which a silver(I) oxide precipitation formed. An ammonia solution (30% in water, few drops) was added drop-wise while the suspension was stirred, until the precipitation was fully dissolved.

B: α-D(+)-glucose (0.24 g) was dissolved in 50 ml water, [α-D(+)-glucose] = 0.58 M.

To produce metallic silver for the electrodes, solutions A and B were mixed in a ratio of 1:1, and pipetted to the target substrate immediately after mixing (covering the cutouts in the masking tape). The mixture, which quickly became dark brown and later gained a metallic shine at its surface, was left for 15 minutes at room temperature on the substrate. Afterwards, the silvering solution was removed, the wafer was rinsed with MilliQ water, and the mask was removed. The wafer then was sonicated for 5 minutes in acetone, then rinsed with acetone, water and 2-propanol and blown dry with pressurized nitrogen to remove any unattached silver particles.

Monolayer graphene on copper foil (synthesized in-house using a hot-wall CVD oven) was spin-coated with a PMMA solution in anisole (6wt% in anisole, Allresist GmbH., AR-P 662.06; 4000 rpm for 60 s), heated at 85 °C for 10 min, and back-etched with oxygen plasma (0.30 mbar, 100 W, 2 min). PMMA-coated graphene on copper was cut to size (3 x 10 mm) and placed floating (Cu-side down) on a bath of an aqueous ammonium persulfate solution (0.2 M); when copper was fully etched, the

PMMA-coated graphene sheet was rinsed by transferring to three MilliQ water baths, then back-fished with the silicon wafer, the graphene sheet stretching across the silver electrodes. Excess water was removed, and the wafer was heated to 150 °C for 15 min. Importantly, the PMMA layer was not removed from graphene.

Using a silver-based electrically conductive epoxy resin (Gentec, EPOTEK EJ2189-LV), copper wires were attached to the silver electrodes and a gate wire was installed to the silicon back side of the wafer, and the wafer was heated to 150 °C to cure the epoxy, which completed the device. Importantly, we chose to produce devices with six electrodes, to eliminate contact resistance by applying the current on electrodes A and F, while measuring the potential between electrodes B & C and D & E; by installing 4 inner electrodes, two transistors could be measured simultaneously to perform the measurements (MEAS, V_{BC}) and (REF, V_{DE}) at the same time.

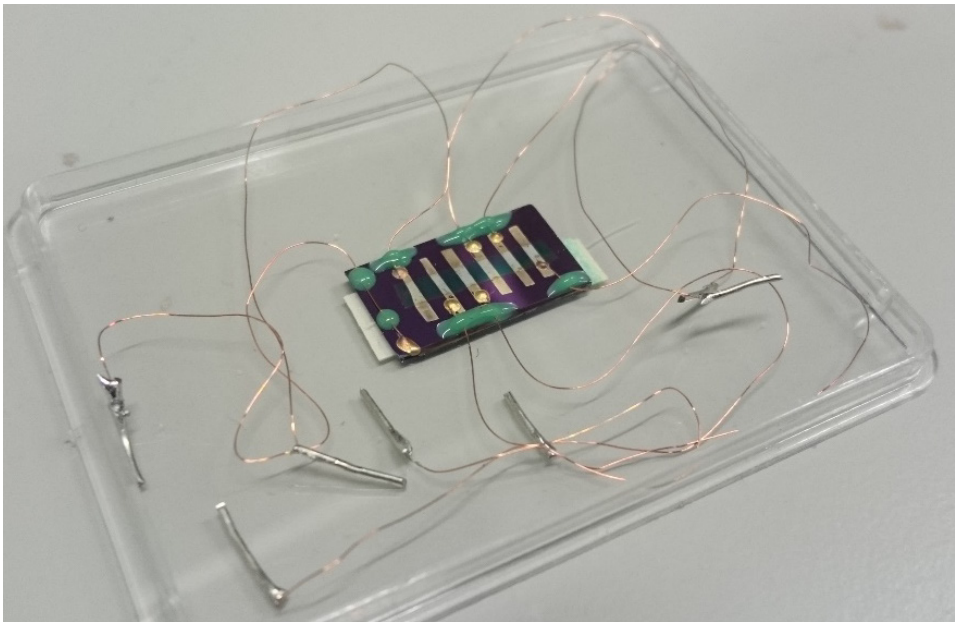

Figure S4.1: Optical photograph of a finished device.

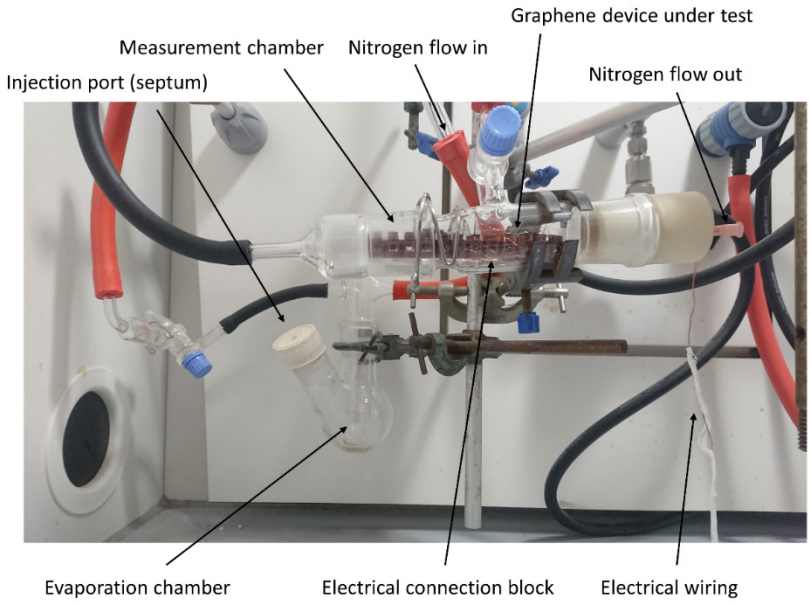

Figure S4.2: Measurement setup for PMMA-coated graphene devices, manual injection.

Table S4.1: List of compounds that were introduced to PMMA-coated graphene devices and numerical values for Peak area A_{norm} (average of 4 manual injections, 10 µl per injection) and standard deviations σ for PMMA-coated and bare GFETs.

		PMMA coated graphene		**Bare graphene**	
#	**compound**	A_{norm}	σ	A_{norm}	σ
1	water	25.18137	55.62705	7.43952	184.66897
2	methanol	73.71028	10.41363	14.21854	110.68771
3	ethanol	8.59934	3.1569	-121.21068	119.97978
4	n-propanol	5.11393	1.20193	62.97931	183.2412
5	i-propanol	11.70176	1.64195	-315.91891	353.11323
6	acetone	15.13339	2.31694	16.81714	154.4035
7	acetonitrile	-20.13984	5.10512	-78.87085	323.05426
8	pentane	0.35825	1.31289	116.39586	85.36589
9	diethyl ether	1.21561	1.91517	33.72192	126.32813
10	thiophene	4.37813	0.99344	-16.49915	373.43897
11	pyrrole	1.74565	0.36542	-203.30179	220.24747
12	pyridine	15.24397	2.01433	973.78835	1139.8853
13	toluene	1.98895	0.19504	134.65172	120.8377
14	anisole	2.1327	0.39652	408.22482	875.3277
15	benzonitrile	1.22257	0.48289	-269.6316	263.27598

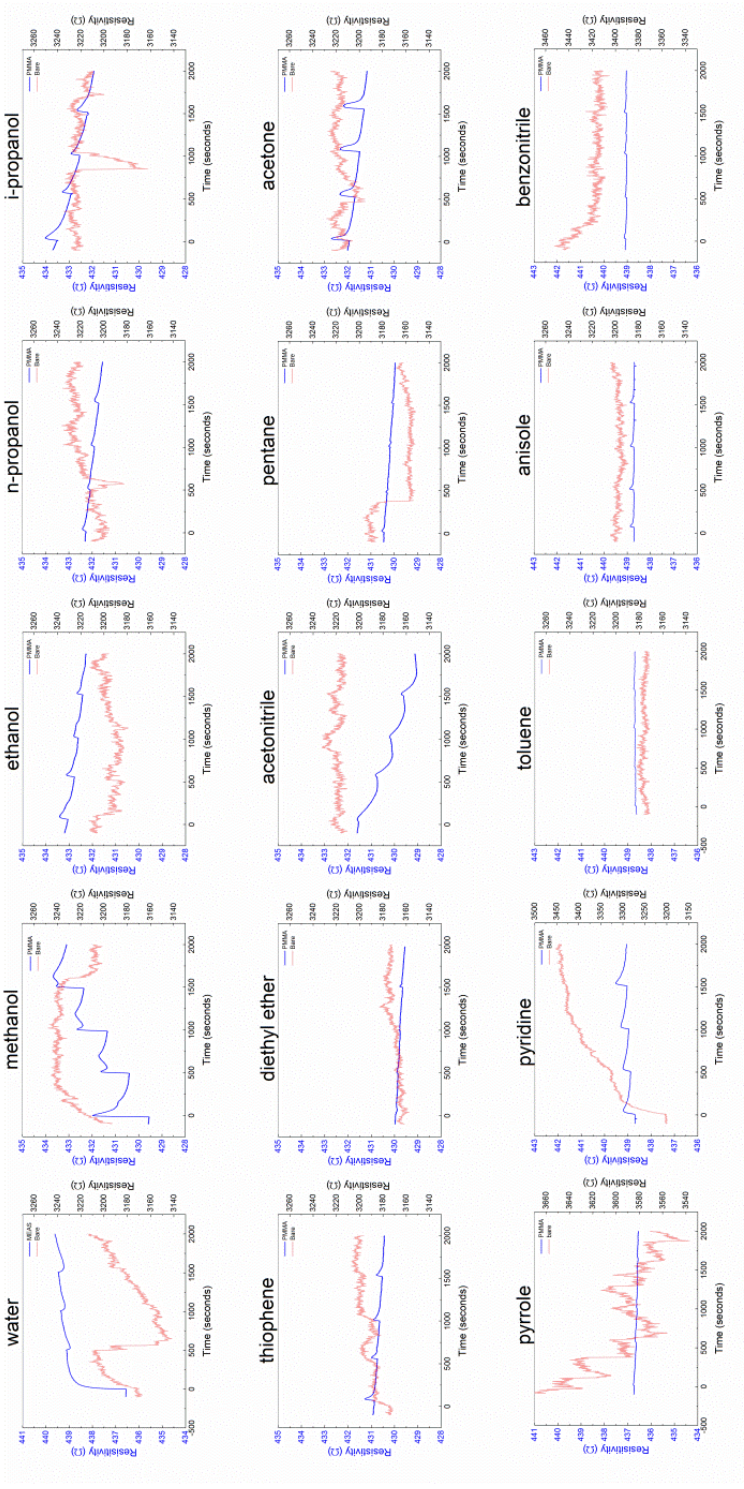

Figure S4.3: Resistivity ρ *vs.* time for graphene-based sensors with a PMMA coating (blue) and without polymer coating (red). Each panel shows a different chemical vapour injection series (4x for each compound). Injections were performed manually with Hamilton gas-tight syringes. The volume of each injection was 10 µl, injections were performed with intervals of 500 s. Resistance was measured continuously throughout the experiments.

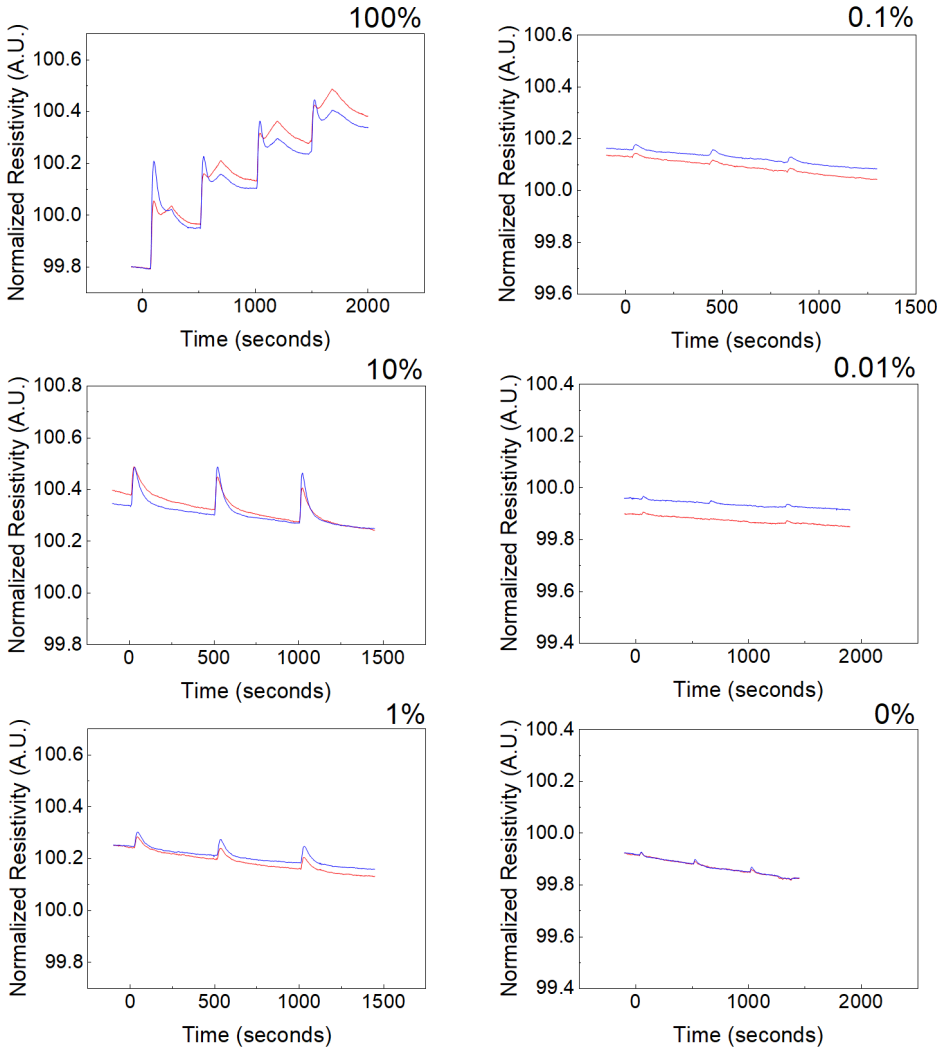

Figure S4.4: Normalized resistivity ρ_{norm} *vs.* time for PMMA-coated graphene sensor. Solutions of methanol in diethyl ether were injected, indicated in v%, 10 µl per injection, with time intervals of 500 s. Percentages are indicated in the top right of each panel. Peak area A_{norm} (average of 4 data points for 100% methanol and 3 data points for other concentrations for duplicate MEAS, V_{BC} and REF, V_{DE} (red and blue, respectively).

Fabrication of Chemical fingerprint (CF) arrays

CF arrays were fabricated with three different individual sensors, denoted CF sensors, combined in a single chamber for simultaneous measurement. CF sensors were fabricated with daughter chips that were obtained from a mother chip. The active components of the CF sensors in the CF array were polymer-coated graphene sheets.

To obtain polymer-coated graphene, monolayer graphene on copper (2x2 cm) grown in house in a hot-wall CVD oven was spin-coated with a 6wt% PMMA solution in anisole, 6wt% CAB solution in anisole, or 5wt% Nafion® 117 solution in aliphatic alcohols (4000 rpm, 500 rpm/s acceleration, 1 minute), heated to 85 °C for 10 min, then etched with O_2 plasma (0.30 mbar, 2 min, 100 W). Notably, all steps described below are the same for PMMA, Nafion® 117 and CAB coated graphene.

To fabricate a mother chip, first of all a silicon wafer chip (30 x 10 mm) was cleaned by sonication in acetone for 5 min. Next, the wafer was rinsed with acetone, MilliQ water and 2-propanol, blown dry with pressurized nitrogen and cleaned with O_2 plasma (Figure S4.5, I). A wafer tape mask with two electrodes cut out (3 mm in width and 20 mm in length, running parallel to the long sides the wafer and separated from each other by 2 mm, II) was applied directly after the plasma treatment for optimal adhesion. A mixture of silvering solution A and B, as described above ("PMMA-coated devices (MEAS & REF)") was placed on the masked wafer; after 15 min at room temperature, the silvering solution was removed and the wafer was rinsed with water. Next, the mask was removed and the wafer was sonicated for 5 minutes in acetone to remove any unattached silver particles, then the wafer was rinsed with acetone, MilliQ water and 2-propanol and blown dry with pressurized nitrogen (III). A polymer-graphene film (4 x 20 mm) on copper was etched with an ammonium persulfate solution (0.2 M), the film was rinsed thrice with MilliQ water by transferring it into successive MilliQ baths, and transferred over the silver electrodes. Importantly, the silver epoxy electrodes were not completely covered by the polymer-graphene film; exposed silver was required for electrical connection later on. After transferring the films, wafers were kept at 45 °C to allow slow evaporation of water from underneath the film; once dry, the wafer was heated to 150 °C for 15 min and cooled to room temperature to obtain a mother chip (IV).

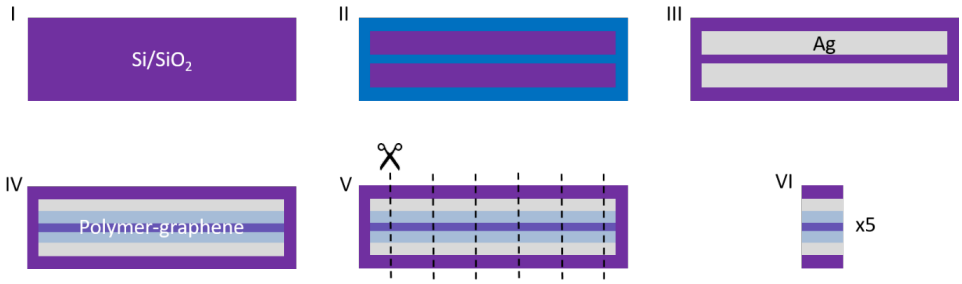

Figure S4.5: Schematic representation of daughter chip fabrication from a mother chip. A long silicon chip (approx. 30x10 mm) was cleaned and treated with O_2 plasma (I), then masked, leaving the electrode areas exposed (II). A silvering solution was placed on the wafer, which deposits metallic silver at the exposed areas, leaving the electrodes after removal of the mask and cleaning (III). Next, graphene was transferred using polymer-assisted transfer (IV). After drying and heating, the wafer was cut by introducing defects in the edge of the wafer and applying pressure (V), giving daughter chips (approx. 3x10 mm) that could be processed into CF sensors (VI).

Daughter chips were obtained by making a scratch on the mother chip and carefully breaking the wafer by applying pressure gently, while not touching the graphene or the silver electrodes (Figure S4.5, V) to obtain a daughter chip which were about 2 to 3 mm wide (VI). CF sensors for the CF array were produced from these daughter chips. Daughter chips could be coated with a PMMA, Nafion® 117 or CAB film; the fabrication process from daughter chip to CF sensor was the same for all

polymers. First, copper wires were taped to a glass slide, three in total. Next, a daughter chip was placed on top of these wires, and the chip was glued in place with Reprorubber epoxy resin (Figure S4.6, I). The copper wires were cut 1 mm away from the edge of the chip and bent towards the chip surface (II). Fresh epoxy resin was then placed at the side of the chip where the wires were bent up to fix them in place (IIIa); the epoxy was still fluid at this point, allowing it to flow under the chip, to fix the wires also at the bottom of the device (IIIb, seen from below). Short heating at 80 °C was applied to cure the epoxy once it completely covered the bottom of the chip. After, excess epoxy resin was removed with a razor blade, as close as possible to the edges of the chip, taking care that the wires were not cut (IV), and any epoxy traces were removed from the wires (V). Next, two wires were connected to the silver electrodes and one gate wire was connected to the silicon back side of the device using a silver-based conductive epoxy resin (VI). Notably, the insulating layer on the wires was not removed beforehand; the bare copper that was exposed by cutting was sufficient for electrical connection. The silver epoxy was cured at 150 °C for 15 min. After cooling to room temperature, the device was carefully removed from the glass slide (VII) to obtain the CF sensor that could be installed in a CF array.

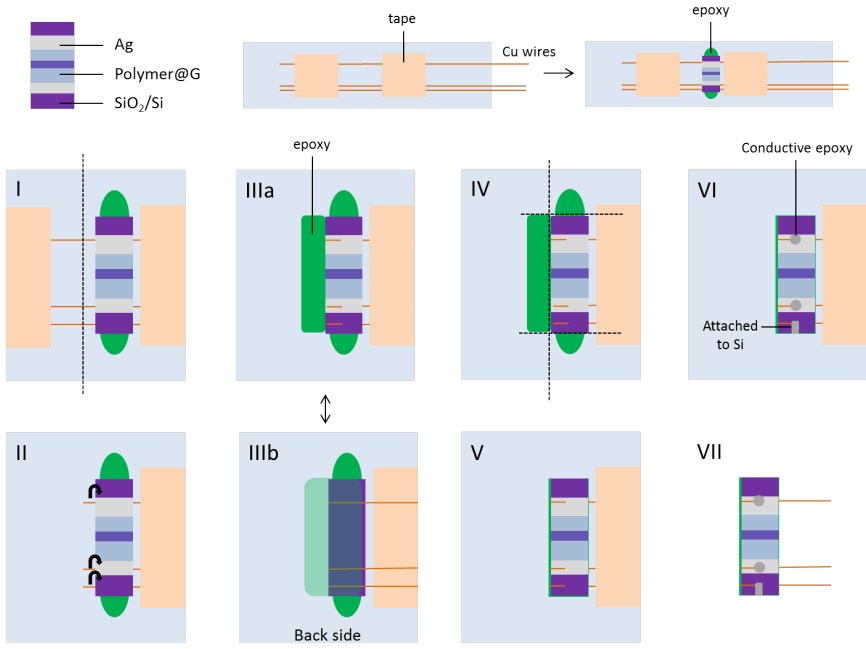

Figure S4.6: Schematic representation of fabrication, step by step, of CF sensors from daughter chips. First, a daughter chip was mounted on a glass slide, which had 3 copper wires taped to it. The daughter chip was placed on the wires and glued to the glass slide with epoxy resin. The wires were cut 1 mm away from the edge of the chip using a razor blade (I; top view), and bent upwards, with two wire ends over the electrodes of the chip and one close to the edge of the chip (II). The bent wires were fixed in position with epoxy resin (IIIa), allowing the resin to flow under the chip (IIIb, seen from below). Excess epoxy was removed with a razor blade (IV), as close as possible to the edges of the chip without damaging the wires (V). Next, the wires were connected to the electrodes (2x) and to the back side of the wafer (1x) using a silver-based conductive epoxy (VI). Finally, the device was removed carefully from the glass slide to obtain the finished CF sensor (VII).

Caps for the CF arrays were produced before installing the CF sensors in a CF array (see Figure S4.7). First of all, the needle (BD microlance™ 3, 18G, 1.2x40 mm, I) from a disposable needle was extracted from the needle base (II), then a separate needle (BD microlance™ 3, 23 G, 0.6x30 mm) was placed in the hole of the needle base (III). The needle base was then filled with Reprorubber epoxy resin while standing upright (IV). After curing at room temperature, the needle was extracted; this left a hole in the epoxy resin (V) through which the cut ends of a GC column (i.d. 0.54 mm, o.d. 0.8 mm) could be inserted to connect the sensor to the GC system (IV).

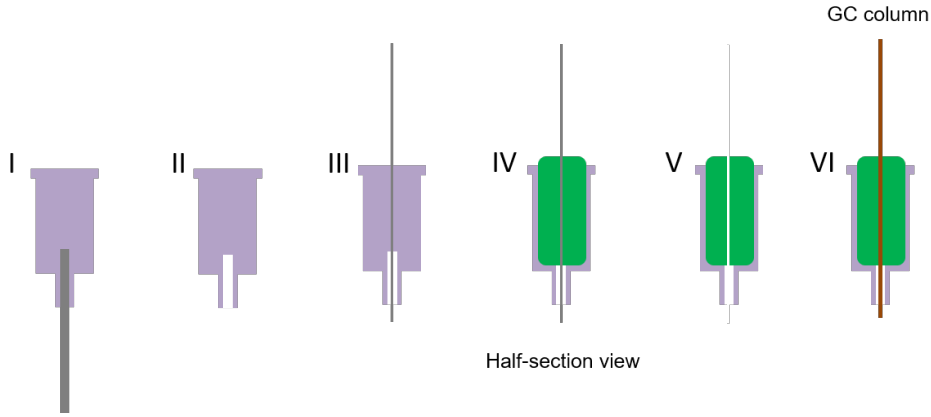

Figure S4.7: Schematic representation of fabrication of CF array caps for integration in a GC system. From a disposable needle (I) the needle was removed (II). Next, a second, thinner needle was placed in the hole that was created (III). Epoxy resin was poured in the needle base (IV), and after the epoxy was cured, the thin needle was extracted to leave a hole in the epoxy (V) through which a GC column fits (VI).

To construct the CF arrays, first of all a PTFE tube (4 cm, i.d. 3 mm, o.d. 3.5 mm) was inserted in a silicone tube (8 cm, o.d 3 mm, o.d. = 4 mm, see Figure S4.8, I). The silicone tube was required for flexibility and for good adhesion of epoxy resins, while the PTFE tube was required for chemical inertness and structural strength. A CF sensor was inserted inside the PTFE tube with their wires run through the two tube walls using a needle (II). This was repeated twice, so three CF sensors with different polymer coatings on graphene (PMMA, Nafion® 117 and CAB) were lined up next to each other inside the PTFE tube (III). Next, the silicone tube was cut to size to fit the sensor caps, which were put into place with Reprorubber epoxy resin (acting as glue and lubricant for their insertion); at the same time the wire holes in the tube were coated with epoxy resin (IV). Next, a thermoplastic sleeve was placed over the silicone tube wall, with the wires running through a hole in this sleeve; the sleeve was then heated shortly with a heat gun to shrink the sleeve to complete the CF array (V). The CF array could be inserted in the GC column by inserting the cut GC column ends through the holes in the sensor caps; this yielded a gas-tight connection as flexible epoxy pushes on the column (the column is wider than the hole in the sensor cap (VI). Wires were connected to an electrical plug for easy connection to the electrical measurement equipment (see Figure S4.9 and Figure S4.10).

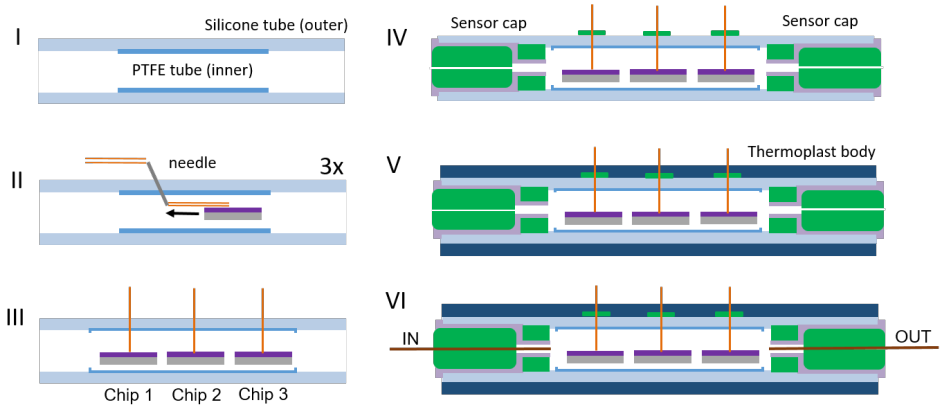

Figure S4.8: Schematic representation of final assembly of a CF array. A PTFE tube was inserted in a silicone tube, leaving about 2 cm of silicone tube on each end (I). CF sensors were inserted in the PTFE tube and their wires were run through the walls of the tubes with a needle (II). Three CF sensors were lined up in the PTFE tube and the tube ends of the silicon tube were cut to fit the sensor caps (III). Sensor caps were installed and fixed with epoxy resin, and the wire holes were patched with epoxy resin (IV). A thermoplastic sleeve was placed around the silicone tube and fixed in place by shrinking using a heat gun (V). The CF array was installed in the GC column by inserting the cut column ends through the sensor caps (VI).

To install the CF arrays in the GC setup (Varian CP3800 Gas Chromatograph, "Svetlana", equipped with auto-injection module Varian CP-8400 Autosampler, "Vladimir") for auto-sampling, the column of the GC (i.d. = 0.54 mm, o.d. = 0.8 mm) was cut ~30 cm away from the injection port of the GC system, creating two ends which could be inserted in the CF array caps (see Figure S4.8, VI). Sliding the column ends into the sensor caps provided a gas-tight connection. Helium was used as a carrier gas at 6 ml/min throughout all experiments; sensors were operated at 30 °C. The temperature of the injection port was 300 °C to ensure complete evaporation of the injected sample. Samples were injected in 1 µl per injection, with a split ratio of 1:40 (*i.e.* one out of 40 parts of the injected volume was introduced to the GC column; the remainder was discarded).

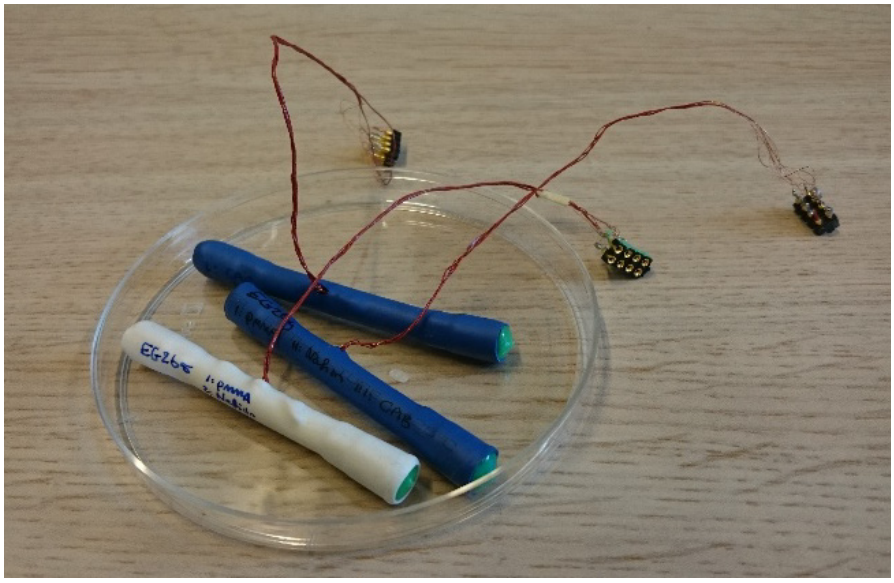

Figure S4.9: Photograph of finished CF arrays. Each tube contains three CF sensors, the wires of which were combined into one electrical plug.

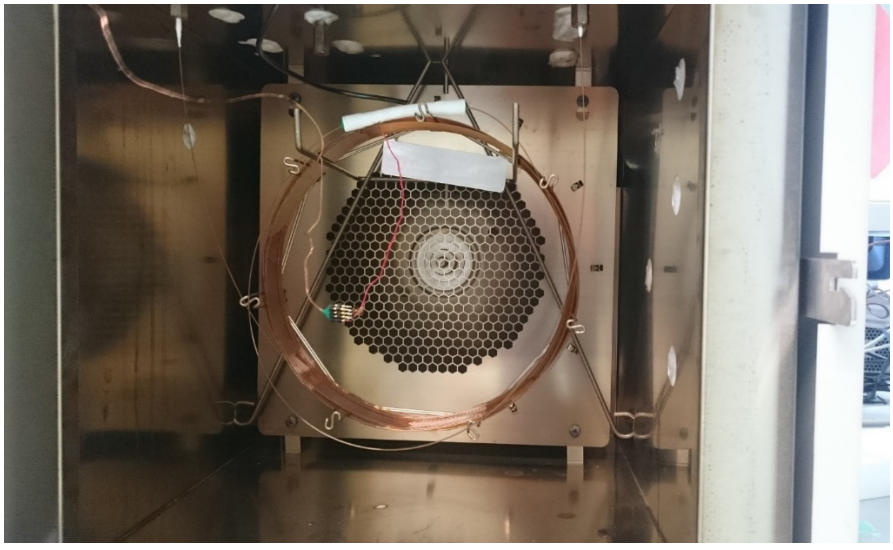

Figure S4.10: A CF array connected inside the oven of the GC system. The sensor is the white tube close to the ceiling of the GC oven; it was connected to the GC column through insertion of the cut ends of the GC column in the sensor caps. The device was electrically connected to the electrical measurement equipment through the plug that was connected to the red wire.

Table S4.2: List of compounds that were introduced to CF arrays.

#	Compound name	#	Compound name
1	acetone	**22**	2,4-pentadione
2	pentane	**23**	cyclopentane
3	diethyl ether	**24**	1-pentene
4	dichloromethane	**25**	1-pentyne
5	chloroform	**26**	2-methyl-2-butanol
6	ethyl acetate	**27**	ethyl acrylate
7	thiophene	**28**	4-pentenoic acid
8	toluene	**29**	1,4-dioxane
9	acetonitrile	**30**	cyclopentanone
10	methanol	**31**	3-methyl-1-butanol
11	ethanol	**32**	1-chlorobutane
12	n-propanol	**33**	1,5-dichloropentane
13	i-propanol	**34**	1-chlorohexane
14	tetrahydrofuran	**35**	1-bromobutane
15	diethyl ketone	**36**	1,4-dibromobutane
16	triethylamine[1]	**37**	1,2-dibromoethane
17	pyrrolidine[1]	**38**	1,3-dibromopropane
18	piperidine[1]	**39**	2,2,2-trifluoroethanol
19	pyridine[1]	**40**	1,1,1,3,3,3,-hexafluoroisopropanol
20	isobutyraldehyde	**41**	ethyl formate
21	butylaldehyde	**42**	nitromethane

[1]: *10v% in pentane*

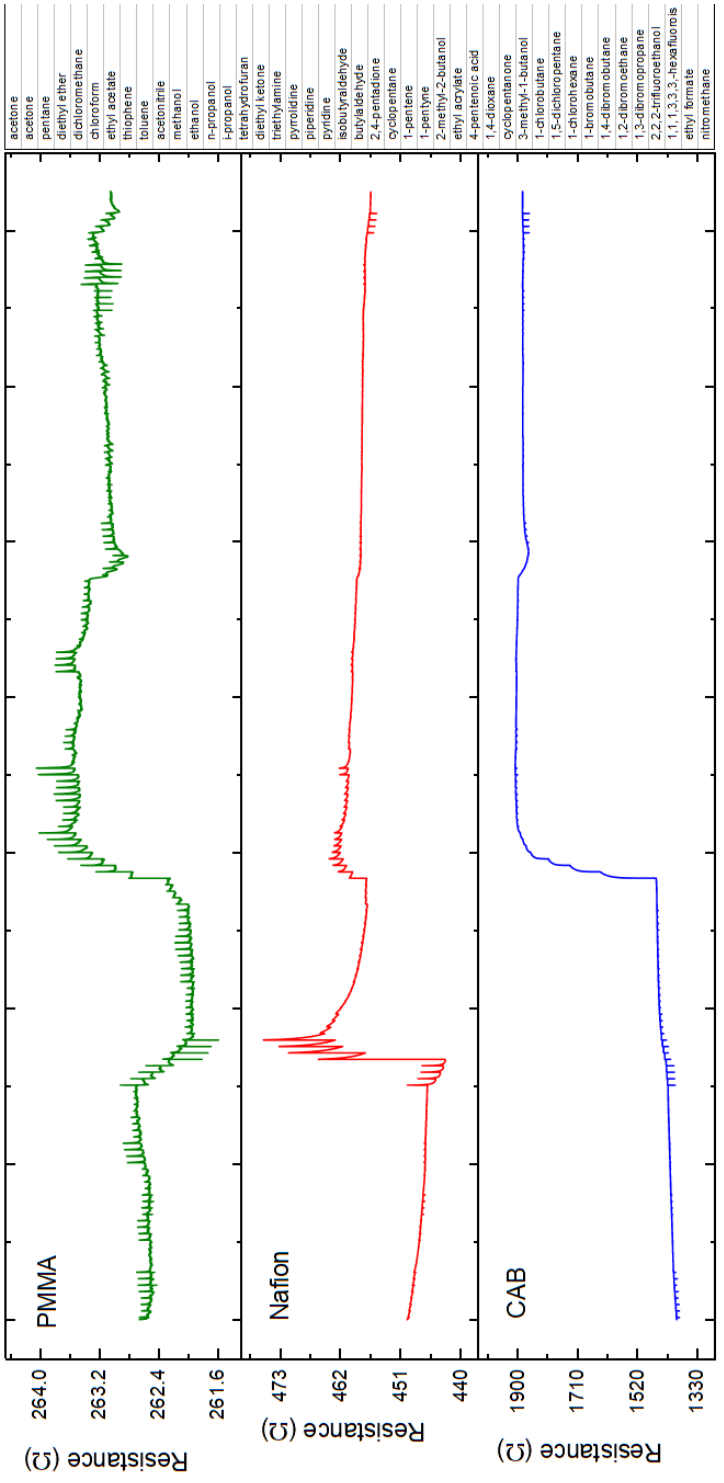

Figure S4.11: Resistance *vs.* time measurement for CF array **1**. The compound injection sequence list is shown on the right, each compound was injected in series of 4 (acetone: 2x4 injections). Time is set to 0 at the first injection of acetone of the second acetone injection series.

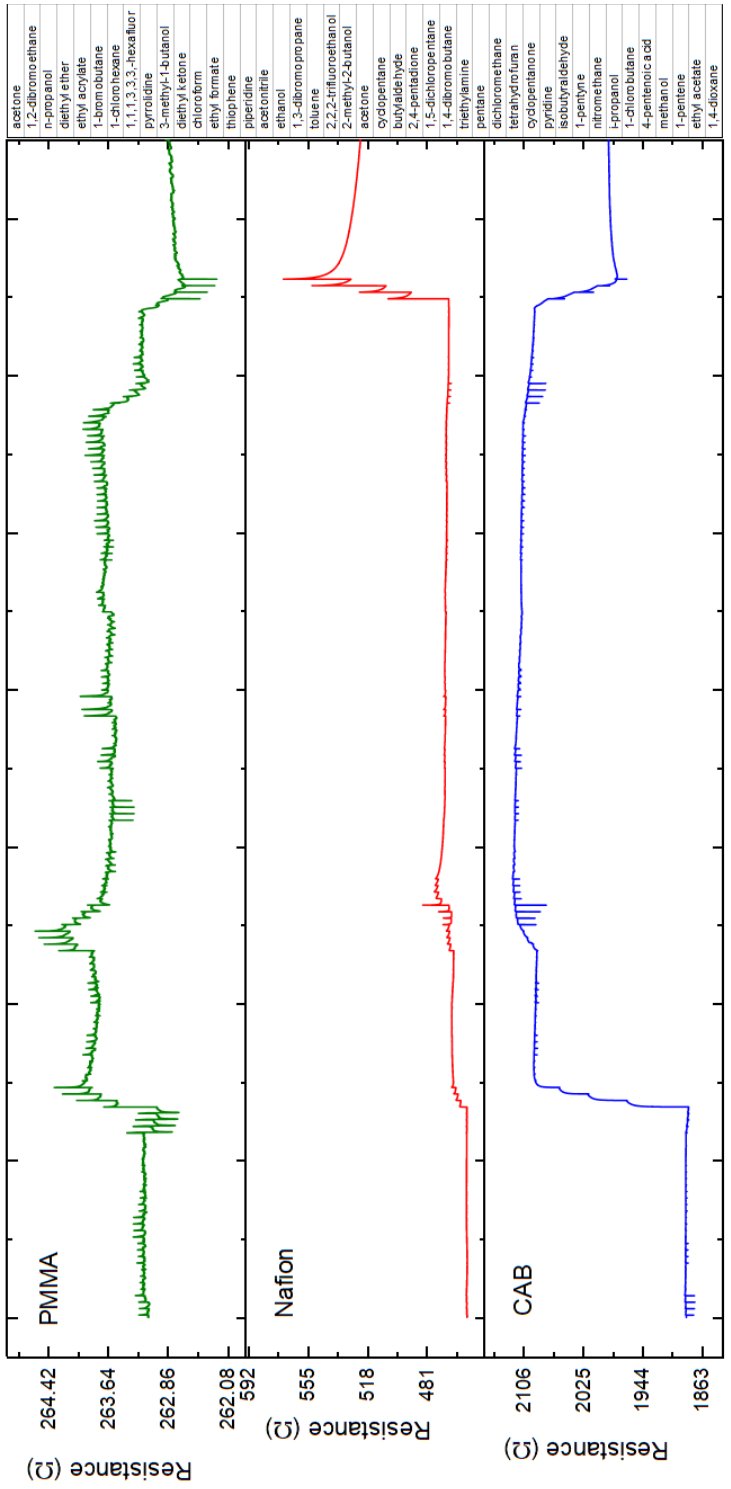

Figure S4.12: Resistance *vs.* time measurement #2 on CF array **1** (polymer coatings are PMMA, Nafion® 117 and CAB, from top to bottom), the sequence of the injected species was randomized (except for the first entry, acetone). Compound injection sequence list is the same for all runs depicted, as shown on the right. Time is set to 0 seconds at first injection of acetone.

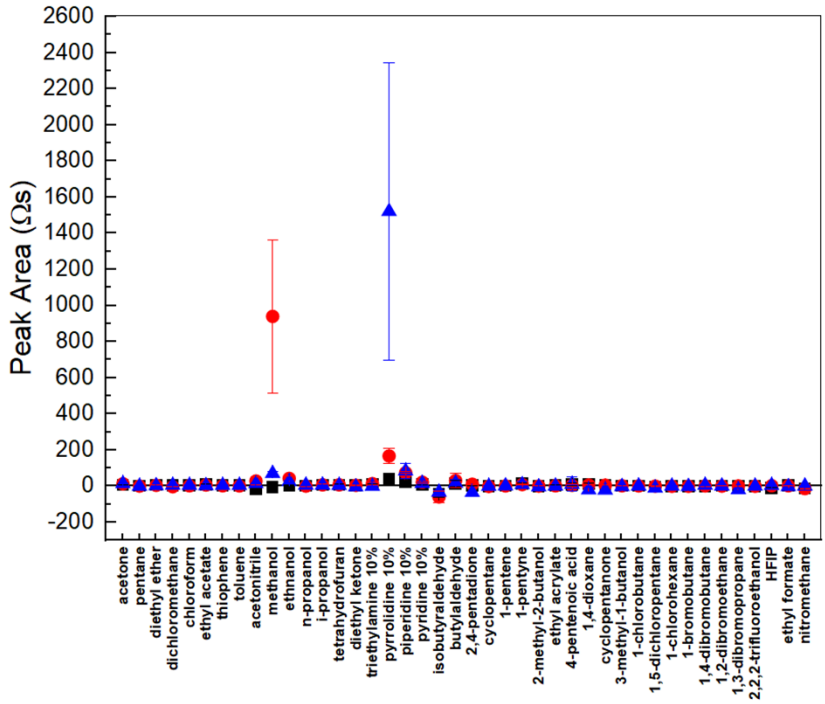

Figure S4.13: Peak area A_{norm} for chemical species, measured with CF array **1** (polymer coatings are PMMA, Nafion® 117 and CAB; black, red and blue, respectively). Peak area values are averages of 4 data points, except for acetone, which is an average of 6 data points.

Table S4.3: Numerical values for Peak area A_{norm} and standard deviations σ for CF array **1**.

	PMMA		Nafion® 117		CAB	
compound	A_{norm}	σ	A_{norm}	σ	A_{norm}	σ
acetone	7.43896	2.78083	12.85827	3.03308	13.56756	0.66049
pentane[1]	1.07157	1.59823	0.41179	1.7257	-0.95157	1.24433
diethyl ether	7.01327	1.32845	4.94156	0.58798	2.15557	1.31364
dichloromethane	3.21905	1.39995	-3.12683	1.30346	4.36031	1.05728
chloroform	3.04386	2.22261	1.76379	1.51299	4.15439	2.62203
ethyl acetate	8.06609	1.16468	6.05993	1.46613	3.24944	1.74872
thiophene	4.54848	2.12179	1.79831	1.06159	4.04566	1.86002
toluene	2.91373	0.59207	1.67848	0.9511	3.54632	0.87343
acetonitrile	-15.1550	1.57902	28.92859	22.92587	13.14771	3.15161
methanol	-5.89378	3.07934	940.4069	423.6901	70.07013	9.2039
ethanol	1.77951	1.81184	43.20043	10.62601	24.47243	4.76745
n-propanol	2.42132	1.90014	0.23445	1.19124	5.97178	3.15219
i-propanol	7.43182	2.04388	7.32022	2.2044	5.70373	3.05182
tetrahydrofuran	7.6041	1.75653	7.48819	1.15154	3.57344	0.83428
diethyl ketone	5.3962	1.70443	4.32261	2.25637	-3.74829	1.70143
triethylamine 10%[1,2]	11.15849	2.15681	14.171	5.54386	-1.09646	1.78713
pyrrolidine 10%[2]	40.54849	17.1272	167.7044	41.94557	1521.101	822.8834
piperidine 10%[2]	25.19245	1.37007	73.69224	5.17681	83.54433	42.26122
pyridine 10%[2]	9.40047	2.39664	22.08471	5.74916	14.99033	4.91891
isobutyraldehyde	-45.4707	17.35695	-59.1565	32.13924	-33.27751	11.4527
butylaldehyde[1]	14.04684	16.48295	31.50854	39.45431	16.51676	17.14666
2,4-pentadione	4.12845	1.98539	10.39429	4.29677	-35.46874	2.66765
cyclopentane	-1.50131	2.32989	-1.20635	2.41638	-1.21685	3.50804
1-pentene[1]	1.19036	2.11041	1.56157	1.55258	1.36114	1.26083
1-pentyne	13.98718	1.64323	9.28235	0.30478	8.08785	16.18646
2-methyl-2-butanol	0.63576	0.7438	0.6625	0.98742	-4.20456	1.56585
ethyl acrylate	2.77418	2.14237	1.76381	2.08929	0.52544	1.65388
4-pentenoic acid	8.96748	7.2974	4.3811	7.43171	9.64439	39.46284
1,4-dioxane	11.78946	5.4758	6.6345	1.18759	-21.3708	13.91718
cyclopentanone	5.33705	0.58355	5.65125	0.95392	-21.90836	1.2401
3-methyl-1-butanol	0.89499	0.96357	1.99293	1.34636	-2.30345	1.40885
1-chlorobutane	1.25859	0.91327	0.96833	0.8763	0.23461	0.8994
1,5-dichloropentane	-2.06434	2.27153	0.56876	2.15016	-10.60375	2.62628
1-chlorohexane[1]	0.67071	1.10135	-0.53106	1.01667	-0.0196	1.4552
1-bromobutane	-0.20781	1.81974	-0.40501	1.08789	-2.19186	1.55078
1,4-dibromobutane[1]	-0.40439	1.93878	1.37309	2.55367	4.82274	1.78403
1,2-dibromoethane[1]	2.0484	1.45638	0.74157	1.46897	0.34492	5.04421
1,3-dibromopropane[1]	-0.38169	2.14108	1.11345	2.53223	-19.77203	5.15564
2,2,2-trifluoroethanol	-1.22238	1.72534	-0.18561	0.87915	-0.24363	0.75251
HFIP[2]	-9.59605	1.16899	1.73615	1.04815	4.15998	1.14245
ethyl formate	3.37347	1.65042	1.91783	1.57161	-3.1243	11.38078
nitromethane	-12.4171	0.94583	-13.03708	2.38556	0.54424	1.51129

[1]: *did not comply with machine learning criterion.*

[2]: *10v% in pentane.*

[3]: *HFIP = 1,1,1,3,3,3,-hexafluoroisopropanol.*

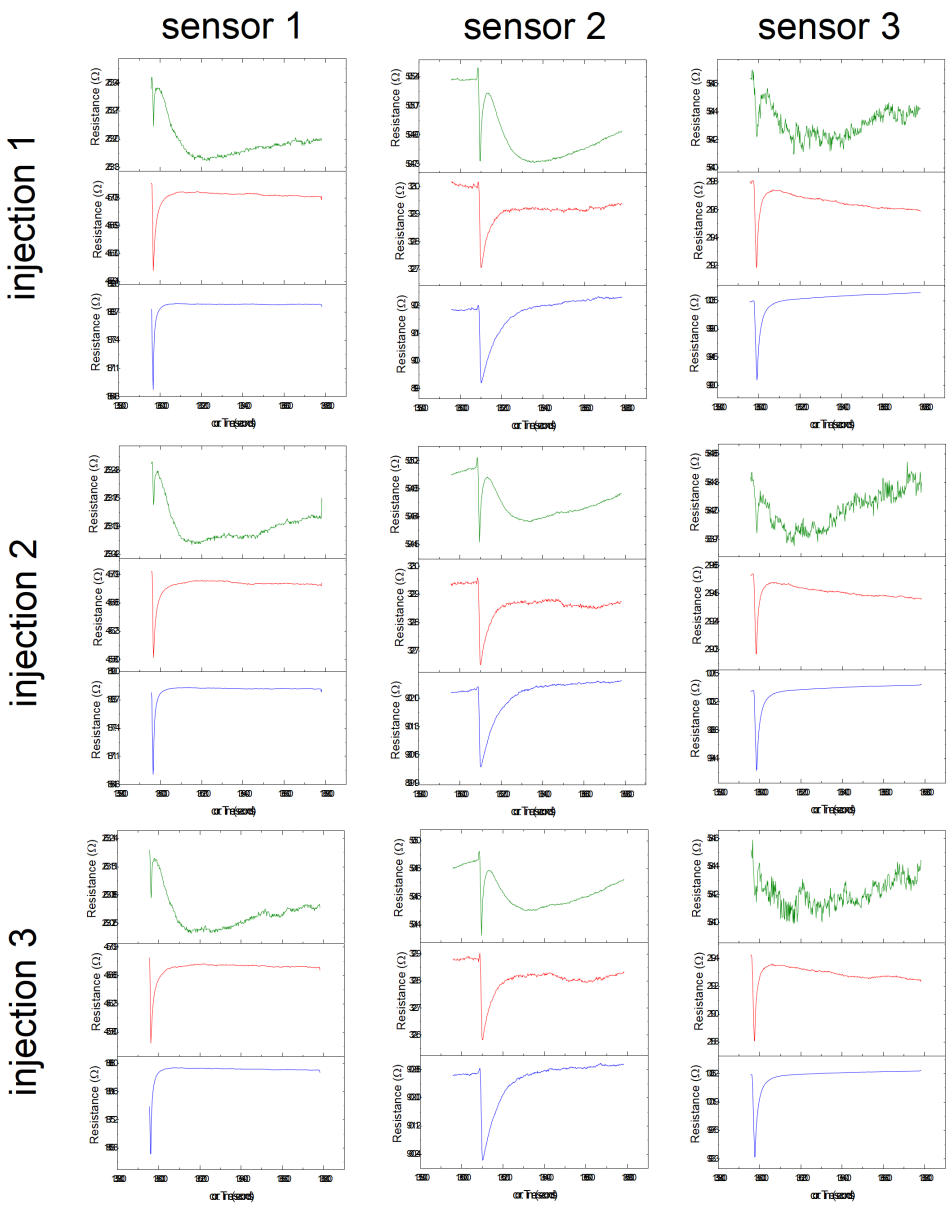

Figure S4.14: Resistance *vs.* time of different CF arrays **1**, **2** and **3** to sequential injections of nitromethane (injections 1 to 3). PMMA-coated sensors is indicated in green, Nafion® 117-coated sensors in red and CAB-coated sensors in blue.

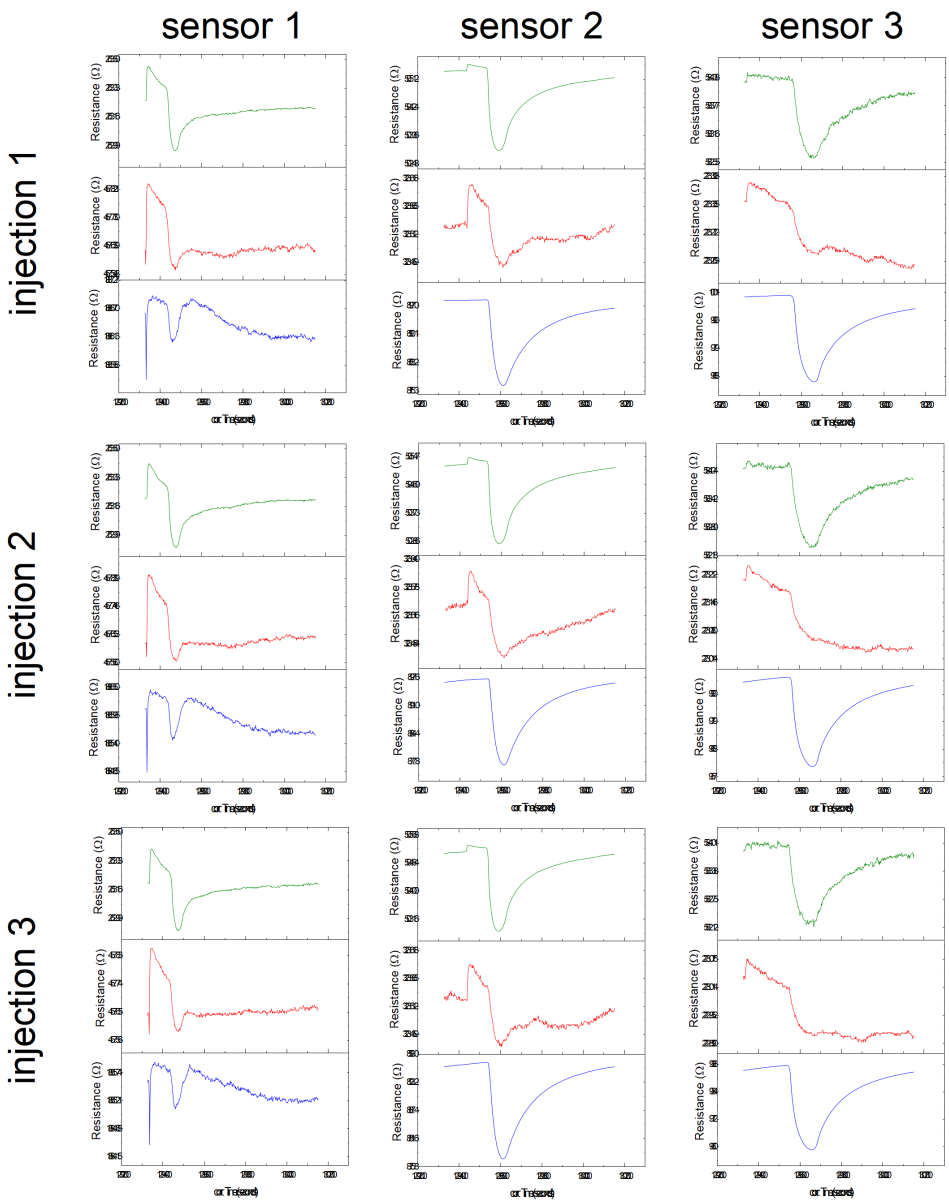

Figure S4.15: Resistance *vs.* time of CF arrays **1**, **2** and **3** to sequential injections of 1,1,1,3,3,3,-hexafluoroisopropanol (HFIP, injections 1 to 3). PMMA-coated sensors is indicated in green, Nafion® 117-coated sensors in red and CAB-coated sensors in blue.

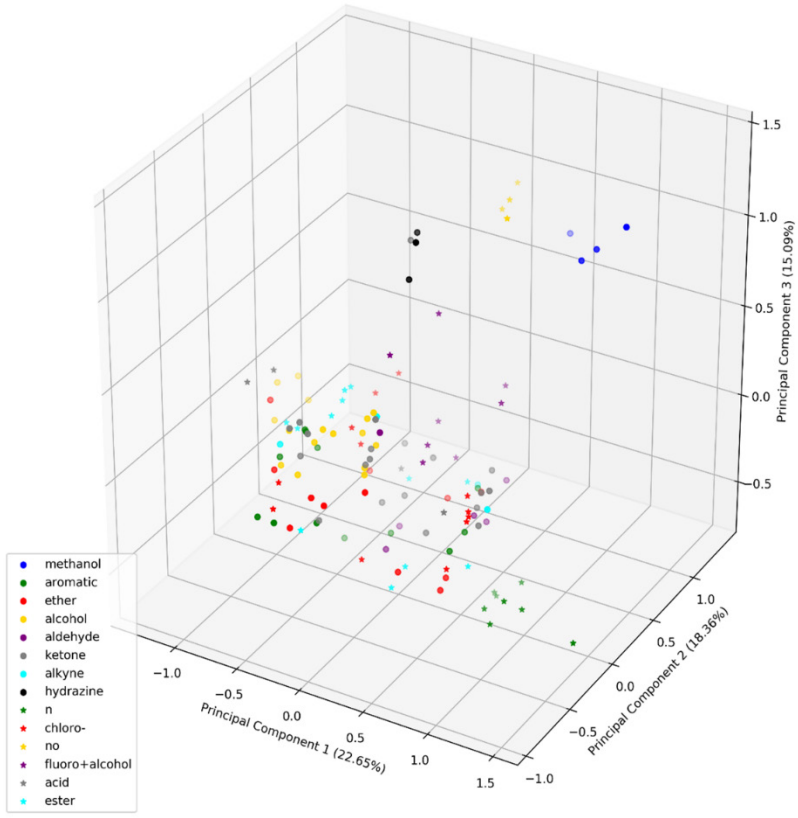

Figure S4.16: Distribution of samples in 3D plot with the first three components of principle component analysis (PCA). The plot was colored and shaped based on which family the compounds belong.

Appendix

Chapter 5

Materials and Methods

All chemicals were purchased from Sigma Aldrich and used without further purification. [Ru(tpy)(biq)Cl]Cl was kindly provided by Dr. Lucien Lameijer.

Regular printing paper (Xerox, 80 gr/m^2, A4) was cut to pieces of 20 x 40 mm. Each piece was soaked with a solution of cellulose acetate butyrate (CAB) in ethyl acetate (30 mg/ml), creating a hydrophilic channel (2 to 3 mm wide) in the center of the paper. After taping the paper with the channel to a microscope slide for support, four electrodes running parallel to the hydrophilic channel, with the inner electrode close to the edges of the channel, were fabricated with conductive silver epoxy (Gentec, EPOTEK EJ2189-LV). The epoxy was cured at 150 °C for 15 minutes. Next, a piece of PMMA-coated graphene (grown by chemical vapor deposition (CVD), monolayer on copper foil; grown in-house in a CVD tube oven), spin-coated with PMMA (6% in anisole, Allresist GmbH., AR-P 662.06; 4000 rpm for 60 s, heated at 85 °C for 10 min, then back-etched in oxygen plasma (0.30 mbar, 100 W, 2 min) was cut to size (2 x 15 mm). The copper underneath the graphene was etched with an ammonium persulfate solution (0.2 M in MilliQ) and the PMMA-graphene film was rinsed by transferring the sheet in three MilliQ baths consecutively, then transferred on the paper, over the electrodes, by fishing the floating film from below. Water was allowed to evaporate at 80 °C, and once dry, the paper was heated for 150 °C for 15 min. Copper wires were placed and fixed to the paper substrate with epoxy resin (Reprorubber Thin Pour) and after curing the epoxy (5 min at 60 °C) the wires were electrically connected to the electrodes on the paper substrate with conductive silver epoxy. The device was heated to 150 °C for 15 min to cure the silver epoxy. Next, a piece of copper foil was cut to size (2 x 10 mm), and a small cut (3 mm) was created in the paper, in the hydrophilic area, perpendicular to the electrodes, away from the graphene. The copper foil was inserted in this cut, to end up underneath the paper supporting the graphene sheet, parallel to the hydrophilic channel. The copper foil was electrically connected to a copper wire with silver epoxy (curing at 150 °C for 15 min) to provide the device with a gate electrode, finishing the device. For wetting the devices, a simple reservoir was made by cutting a plastic syringe and fitting a plastic pipetting tip in the nozzle; the liquid was loaded in the pipetting tip which touched the device on the hydrophilic channel.

Oxygen plasma was generated using a capacitively coupled plasma system with radio-frequency of 40 kHz and 200 W power from Diener electronic (Femto), employed at room temperature. Spin coating was done with a POLOS SPIN150i tabletop spin coater. Optical images were obtained using a Leica DM2700 M Brightfield microscope fitted with Leica MC120 HD camera. Electrical characterization of devices was performed inside a closed steel box (with BNC connectors) using a Keithley Sourcemeter model 2450 and 2400 in combination with Kickstart measuring software. The gate voltage was supplied using a Keithley Sourcemeter (model 2450) as well; both Sourcemeters were earthed on the same point. Green light irradiation (530 nm) was done using a high-power LED (Roithner Lasertechnik, H2A1-H530) operated at 350 mA with optical power P = 8.15 mW, which was installed in the lid of the measurement box (~3 cm away from the GFET on paper device).

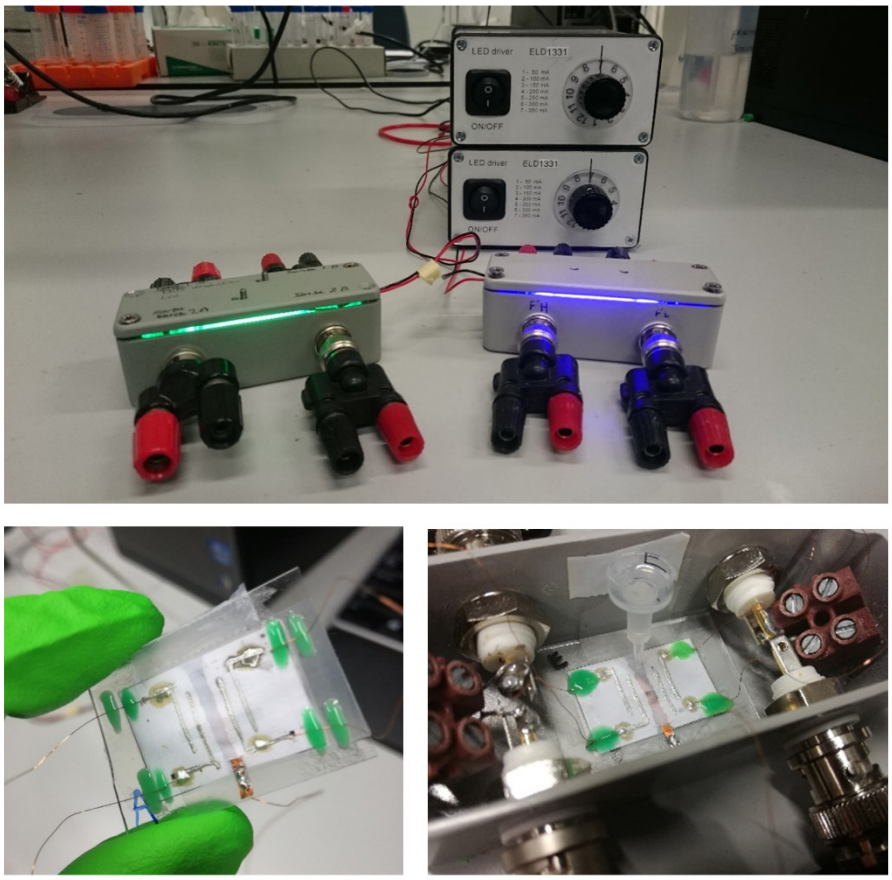

Figure S5.1: Photographs of the measurement setup (top, two setups are shown here with a green and blue LED), a finished GFET on paper (bottom left, without liquid reservoir), and a device installed in the measurement box, with the reservoir (bottom right).

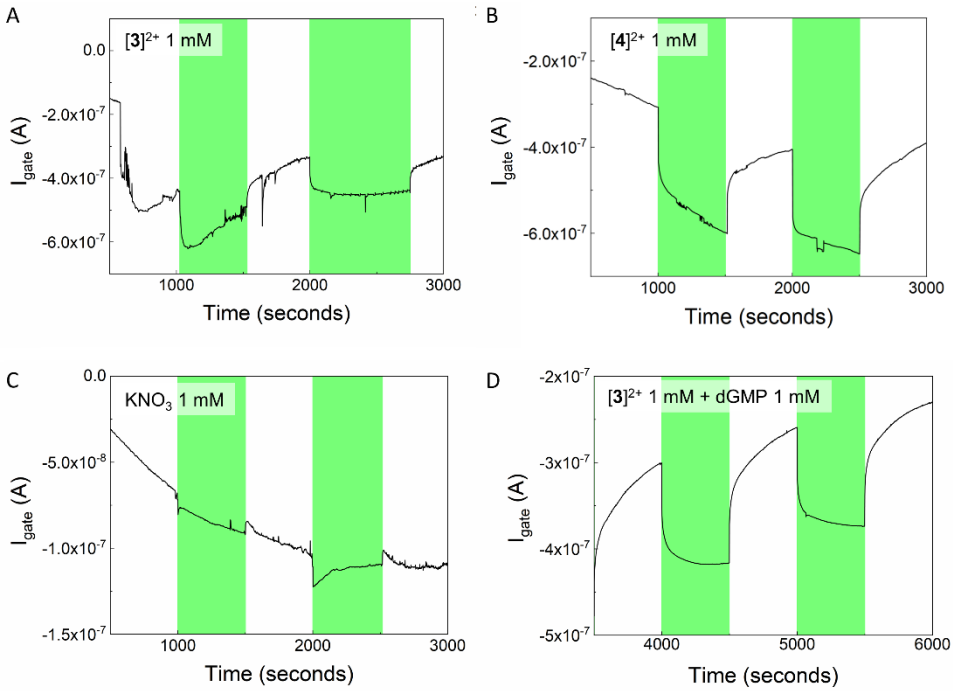

Figure S5.2: Leak current I_{gate} *vs.* time in the dark (white regions) and under irradiation conditions (green regions, 530 nm, P = 8.15 mW) for GFETs on paper wetted with A) a solution containing [**3**]$^{2+}$ made from [**1**]Cl (1 mM) in water, B) [**4**]Cl_2 (1 mM) in water, C) KNO_s (1 M) in water, and D) a solution containing [**3**]$^{2+}$ (1 mM) and dGMP (1 mM). R was measured between electrodes *B* and *C*, while a potential was applied on *A* and *D*, V_{AD} = 250 mV.

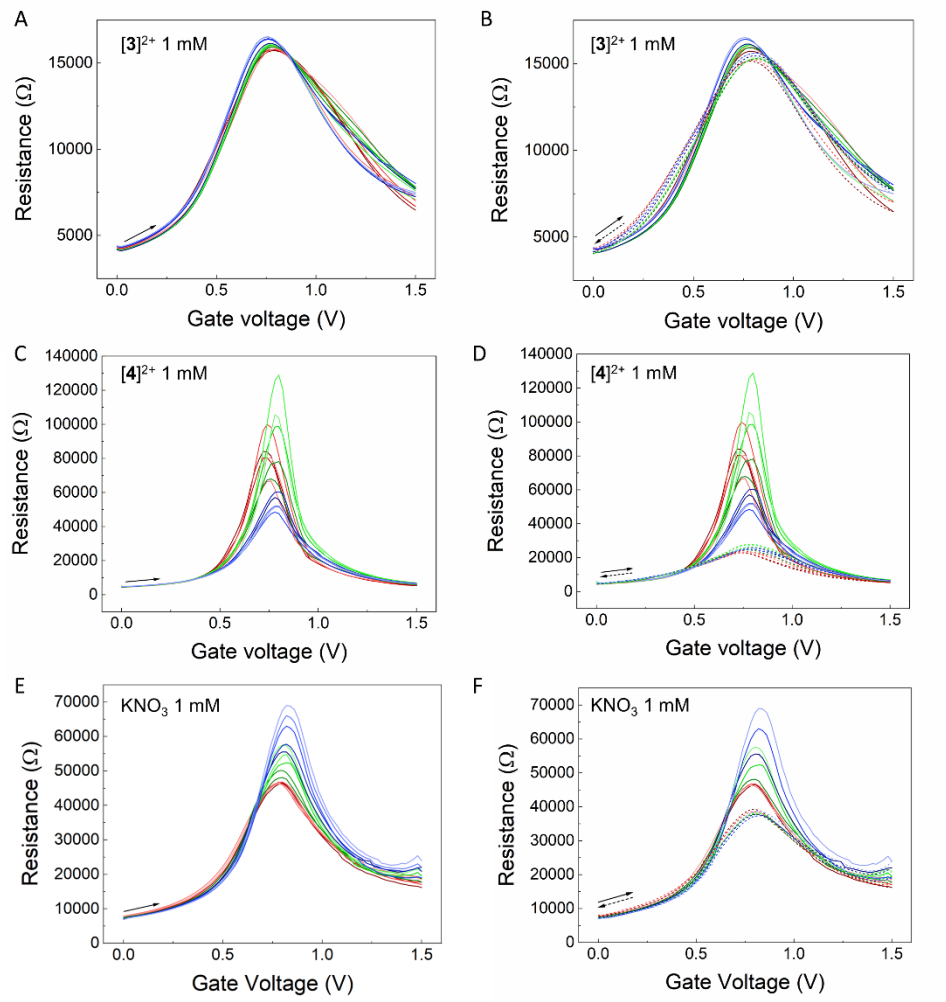

Figure S5.3: *R vs.* V_{gate} during forward sweeps (0 – 1.5 V) and overlay of forward (solid lines) and backward sweeps (dashed lines) for devices wetted with [**1**]Cl (hydrolyzed into [**3**]$^{2+}$, 1 mM, A-B), [**4**]Cl_2 (1 mM, C-D), or KNO_3 (1 mM, E-F). Starting in the dark (state I, red lines), a typical device was irradiated with green light (530 nm, P = 8.15 mW, state II, green lines), back to dark (state III, blue lines). After 10 dark stabilization cycles, 5 V_{gate} cycles were recorded for each state between 0 and 1.5 V, which are shown as their corresponding dark to light colors (dark to light red lines for state I, etc.), solid/dashed line indicates forward/backward sweep, respectively, with a sweeping rate of 0.02 Vs^{-1}. R was measured between electrodes B and C, while a potential was applied on A and D, V_{AD} = 250 mV.

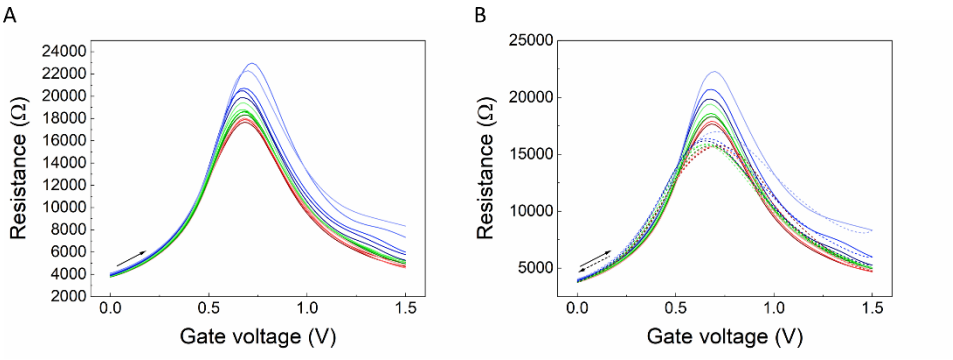

Figure S5.4: *R vs.* V_{gate} during forward sweeps (0 – 1.5 V, A) and overlay (B) of forward (solid lines) and backward sweeps (dashed lines) for devices wetted with **[3]**$^{2+}$ (1mM) + dGMP (1 mM). Starting in the dark (state I, red), the device was irradiated with green light (530 nm, P = 8.15 mW, state II, green line), back to dark (state III, blue line). After 10 dark stabilization cycles, 5 V_{gate} cycles were recorded for each state between 0 and 1.5 V, which are shown as their corresponding dark to light colors (dark to light red for state I, etc.), solid/dashed line indicates forward/backward sweep, varied at 0.02 Vs^{-1}. R was measured between electrodes B and C, while a potential was applied on A and D, V_{AD} = 250 mV.

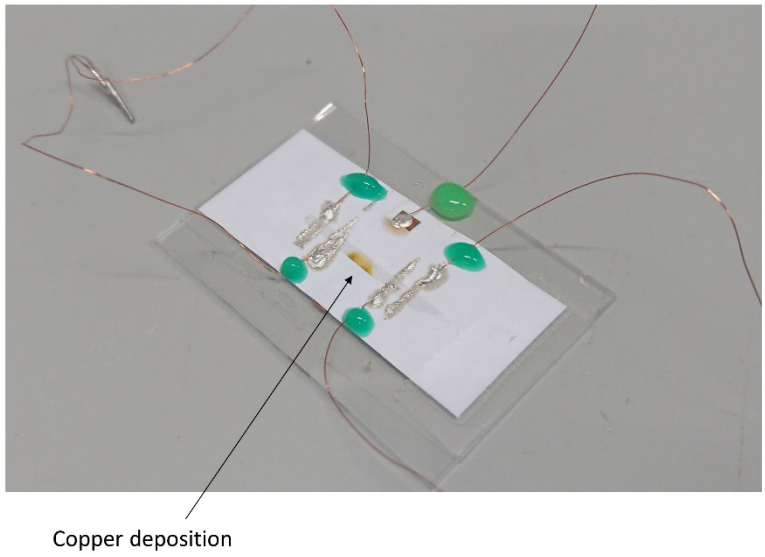

Figure S5.5: Deposition of solid copper on graphene for a GFET on paper that was wetted with KNO_3 (1 mM) and used in a gate cycling experiment (0 – 1.5 V, 15 cycles; cycle 1 to 5 and 10 to 15 in the dark, and cycle 6 to 10 under green light irradiation, 530 nm, P = 8.15 mW).

Appendix

Chapter 6

Materials and methods

All chemicals were purchases from Sigma Aldrich and used without further purification. λ-DNA (from *E. coli* bacteriophage λ, 48502 base pairs) was purchased at Sigma Aldrich (D9780-1MG, USA). When required, solvents were dried over activated molsieves (4Å) and deoxygenated by nitrogen bubbling. Reactions were performed under inert nitrogen atmosphere using standard Schlenk techniques. [Ru(tpy)(biq)Cl]Cl, compound [**1**]Cl, was prepared according to a previously reported method.[1] $[Ru(tpy)(biq)(OH_2)]^{2+}$, compound $[\mathbf{2}]^{2+}$, was obtained by dissolving [**1**]Cl in water.

Silicon nitride chips with a 30 nm thick membrane were used for nanopore drilling with dielectric breakdown by applying a potential between the *cis* and *trans* chamber that were filled with electrolyte solution (1 M KCl). The potential was applied with a pulse generator while measuring the resistance between the *cis* and *trans* chamber. When the resistance between the chambers dropped strongly, the hole was created and the potential over the membrane was removed and the nanopore could be used for DNA detection. All experiments were done in 1 M KCl buffered with 10 mM Tris and 1 mM EDTA. λ-DNA (10 ng/μL), was introduced in the *cis* chamber of the nanopore device, which moved to the *trans* chamber through the nanopore, driven by an electrostatic potential of -100 mV. Analysis of the ion current traces was done with Transalyzer software.[2]

Photochemistry

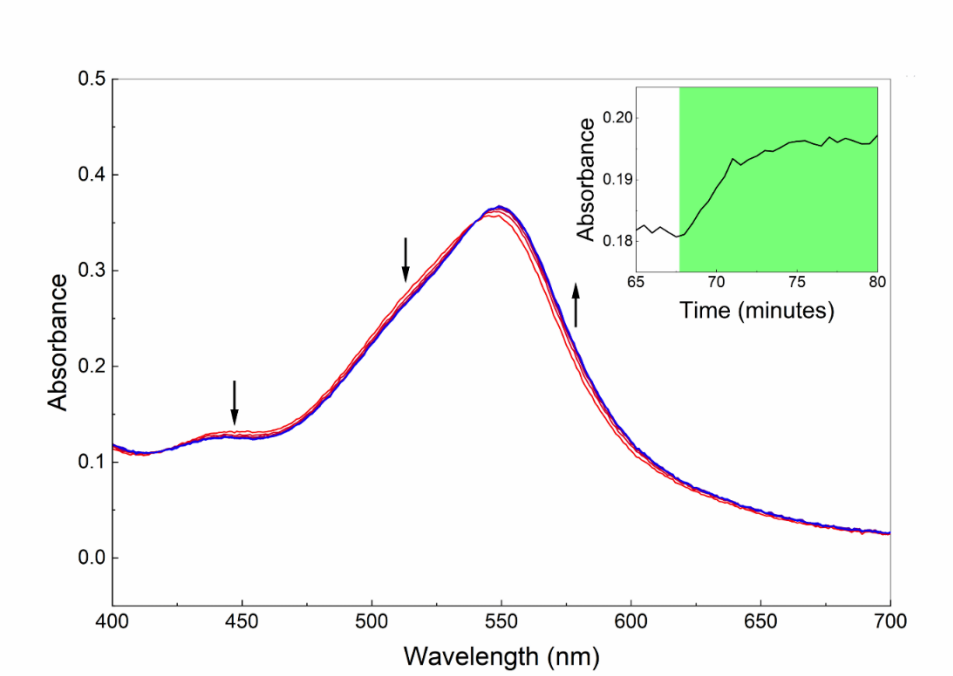

Figure S6.1: UV-vis spectra of 50 μM [**1**]Cl + 250 μM dGMP at 37 °C. Solution was kept in the dark (red), then irradiation was started (530 nm) and spectra were recorded every 2 minutes, until the conversion was complete (blue). Inset: evolution of the absorbance at 580 nm, either in the dark (white region) or upon irradiation with 530 nm light (green region, photon flux = 1.36 x 10^{-7} mol·s^{-1}).

References and notes

[1] L. N. Lameijer, D. Ernst, S. L. Hopkins, M. S. Meijer, S. H. C. Askes, S. E. Le Dévédec, S. Bonnet, *Angew. Chem., Int. Ed.* **2017**, *56*, 11549.

[2] C. Plesa, C. Dekker, *Nanotechnology* **2015**, *26*, 084003.

Appendix

Chapter 7

Materials and methods

All chemicals were purchases from Sigma Aldrich and used without further purification. [Ru(tpy)(biq)Cl]Cl was prepared according to a previously reported method.[1] If required, solvents were dried over activated molsieves (4 Å) and deoxygenated by nitrogen bubbling. Reactions were performed under inert nitrogen atmosphere using standard Schlenk techniques.

Synthesis

4′-(3-hydropropoxy)-2,2′:6′,2′′-terpyridine (**2**)

Compound **2** was prepared according to a modified literature procedure.[2] In a round bottom flask under nitrogen atmosphere, 1,3-propanediol (1.4 ml, 21 mmol) was dissolved in dry DMSO (25 ml). While the solution was stirred, powdered KOH (1.0 g, 18 mmol) was added and the mixture was heated up to 60 °C for 10 min. 4′-Chloro-terpyridine (0.96 g, 3.6 mmol) was added and the temperature was maintained at 60 °C. After 5 h, the mixture was cooled down to RT and diluted with ice cold water (50 ml). The pH was adjusted to 6 with 1 M HCl solution. The compound was extracted with ethyl acetate (3 x 25 ml) and the combined organic layer was washed with water and brine (both 3 x 25 ml) to remove DMSO. The organic layer was dried over $MgSO_4$ and the solvent was evaporated to obtain compound **2** as a white solid (824 mg, 2.64 mmol, 75%).

Analysis corresponded to the published data. For information:

^{1}H NMR (400 MHz, chloroform-*d*): δ (ppm) 8.68 (d, *J* = 4.8, 1.8, 0.9 Hz, 2H, 4), 8.61 (d, *J* = 7.9, 1.1 Hz, 2H, 1), 8.03 (s, 2H, 5), 7.86 (t, *J* = 7.7, 1.8 Hz, 2H, 3), 7.34 (t, *J* = 7.5, 4.8, 1.2 Hz, 2H, 2), 4.41 (t, *J* = 6.1 Hz, 2H, α), 3.89 (t, *J* = 5.9 Hz, 2H, γ), 2.12 (p, *J* = 6.0 Hz, 2H, β).

LC-MS (MeOH): *m*/*z* (calc) 308.2 (308.14, [**2**+H]$^+$), 637.2 (637.25, [2×**2** +Na]$^+$).

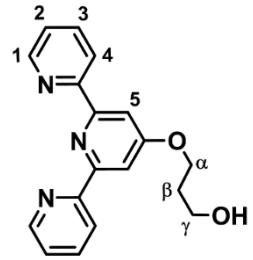

3-([2,2′:6′,2″-terpyridin]-4′-yloxy)propyl-4-(pyren-1-yl)butanoate (**3**)

Compound **3** was prepared using a modified literature procedure.[3] A mixture of 1-pyrenebutyric acid (616 mg, 2.14 mmol), **2** (590 mg, 1.92 mmol) and 4-(dimethylamino)pyridine (DMAP, 233 mg, 1.91 mmol) in anhydrous DCM (6 ml) was cooled to 0 °C and dicyclohexylcarbodiimide (DCC, 540 mg, 2.62 mmol) in anhydrous DCM (6 ml) was added. The reaction mixture was first stirred for 10 min at 0 °C, then overnight at room temperature. The precipitated dicyclohexylurea was removed by filtration over Celite. The filtrate was washed with water (3x 10 ml) and saturated $NaHCO_3$ aqueous

solution (3 x 10 ml). The organic layer was dried over anhydrous $MgSO_4$ and filtrated. The filtrate was evaporated by rotary evaporation. The product was then crystallized from chloroform, using methanol as a counter-solvent, to give compound **3** as an off-white solid (494 mg, 0.86 mmol, 45%).

^{1}H NMR (500 MHz, chloroform-*d*): δ (ppm) 8.66 (d, *J* = 4.8, 2H, 4), 8.57 (d, *J* = 7.9, 2H, 1), 8.26 (d, *J* = 9.2 Hz, 1H, 13), 8.13 (m, 2H, 8 + 10), 8.09 – 8.03 (m, 2H, 7 + 14), 8.03 (s, 2H, 5), 7.99 (s, 2H, 11 + 12), 7.96 (t, *J* = 7.6 Hz, 1H, 9), 7.84 – 7.78 (m, 3H, 2 + 6), 7.29 (t, *J* = 7.5 Hz, 2H, 3), 4.35 – 4.27 (m, 4H, α + γ), 3.36 (t, *J* = 7.7 Hz, 2H, δ), 2.48 (t, *J* = 7.2 Hz, 2H, ζ), 2.24 – 2.14 (m, 4H, β + ε).

^{13}C NMR (126 MHz, chloroform-*d*): δ (ppm) 173.5 (C_q), 167.1 (C_q), 157.2 (C_q), 156.1 (C_q), 149.1 (4), 136.8 (2), 135.7 (C_q), 131.5 (C_q), 132.0 (C_q), 130.0 (C_q), 128.8 (C_q), 127.6 (11), 127.7 + 127.5 (6 + 7), 126.8 (12), 125.9 (9), 125.1 (C_q), 125.1 (C_q), 124.9 + 124.9 + 124.9 (8, 10, 14), 123.9 (3), 123.4 (13), 121.4 (1), 107.4 (5), 64.6 (α) + 61.0 (γ), 33.9 (δ), 32.8 (ζ), 28.5 (β), 26.8 (ε).

LC-MS (acetone): *m*/*z* (calc.) 578.0 (578.24, [**3** + H]$^+$), 600.1 (600.23, [**3** + Na]$^+$).

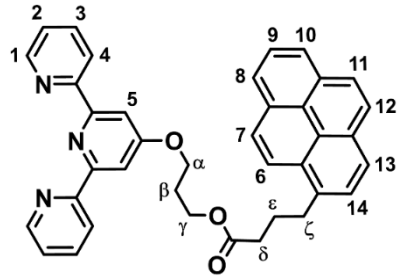

Ruthenium dimer [Ru(**3**)Cl$_2$]$_2$ ([**4**])

Compound [**4**] was prepared using an adapted literature procedure.[4] In a 3-neck round-bottom flask equipped with dropping funnel and nitrogen flow, [Ru$_2$Cl$_2$(*p*-cymene)$_2$] (55 mg, 0.090 mmol) was dissolved in deoxygenated DCM (5 ml). A solution of **3** (100 mg, 0.17 mmol) in deoxygenated DCM (5 ml) was transferred to the dropping funnel, and added to the mixture over 60 min at RT. Next, the reaction mixture was filtered through a Whatman membrane filter (0.2 μm pore size) and [**4**] was obtained as a purple solid (91 mg, 0.061 mmol, 68%).

^{1}H NMR (500 MHz, DMSO-d_6): δ (ppm) 9.36 (d, *J* = 5.4 Hz, 4H, 4), 8.61 (d, *J* = 8.2 Hz, 4H, 1), 8.40 (d, *J* = 9.3 Hz, 2H, 13), 8.35 (s, 4H, 5), 8.26 (d, *J* = 7.6 Hz, 4H, 8, 10), 8.21 (d, *J* = 4.3 Hz, 2H, 14), 8.19 (d, *J* = 2.8 Hz, 2H, 7), 8.11 (d, *J* = 0.6 Hz, 4H, 11+12), 8.04 (t, *J* = 7.6 Hz, 2H, 9), 7.96 – 7.91 (m, 6H, 2 + 6), 7.49 (t, *J* = 7.3 Hz, 4H, 3), 4.50 (t, *J* = 6.2 Hz, 4H, α), 4.31 (t, *J* = 6.3 Hz, 4H, γ), 3.37 (t, *J* = 8.3 Hz, 4H, δ), 2.52 (m, overlap with DMSO peak, ζ), 2.22 (p, *J* = 6.2 Hz, 4H, β), 2.07 (p, *J* = 7.5 Hz, 4H, ε).

LC-MS (MeOH): *m*/*z* (calc.) 792.1 (792.63, [(Ru(**3**)Cl(DMSO))$_2$]$^{2+}$), 870.1 (870.14, [Ru(**3**)Cl(DMSO)$_2$]$^+$).

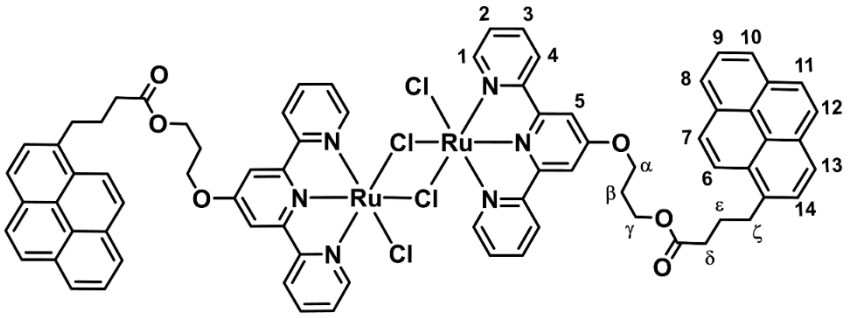

[Ru(biq)(**3**)Cl]Cl ([**5**]Cl)

[**5**]Cl was prepared using a modified literature procedure.[1] Dimer [**4**] (90 mg, 0.060 mmol) was dissolved in deoxygenated ethylene glycol (0.75 ml) and 2,2′-biquinoline (33 mg, 0.13 mmol) was added. The mixture was heated up to 180 °C under a nitrogen atmosphere. After 2.5 h, the reaction mixture was diluted with ethanol (1.5 ml), and filtered over Celite to remove insoluble impurities. Ethanol was removed by rotary evaporation and Et_2O was added (25 ml) to the residue, resulting in a precipitate which was washed with Et_2O (3 x 25 ml) and filtered with a Whatman membrane filter (0.2 μm pore size). The obtained dark purple/blue solid was dissolved in methanol (5 ml) and a precipitation was formed by adding diethyl ether (50 ml), which after filtration, washing with ether (3 x 25 ml) and drying yielded [**5**]Cl (86 mg, 0.085 mmol, 71%).

^{1}H NMR (500 MHz, chloroform-*d*): δ 9.67 (d, *J* = 8.7 Hz, 1H, 15), 8.86 (d, *J* = 8.8 Hz, 1H, 20), 8.67 (d, *J* = 8.8 Hz, 1H, 19), 8.57 (d, *J* = 8.8 Hz, 1H, 21), 8.52 (d, *J* = 8.1 Hz, 2H, 4), 8.31 (d, *J* = 9.2 Hz, 1H, 14), 8.26 (s, 2H, 5), 8.14-8.10 (m, 2H, 8, 10), 8.10-8.04 (m, 4H, 18, 7, 13, 22), 7.98 (s, 2H, 11, 12), 7.95 (t, *J* = 7.6 Hz, 1H, 9), 7.86 (d, *J* = 7.8 Hz, 1H, 6), 7.81 (t, *J* = 8.7 Hz, 1H, 16), 7.77 (t, *J* = 8.0 Hz, 1H, 17), 7.68 (t, *J* = 7.8 Hz, 2H, 3), 7.63 – 7.57 (m, 3H, 1, 23), 7.30 (t, *J* = 8.0 Hz, 1H, 24), 7.20 (t, *J* = 8.7 Hz, 1H, 25), 7.05 (t, *J* = 6.8 Hz, 2H, 2), 6.79 (d, *J* = 8.9 Hz, 1H, 26), 4.71 (t, *J* = 5.9 Hz, 2H, α), 4.39 (t, *J* = 6.7 Hz, 2H, γ), 3.40 (t, *J* = 7.4 Hz, 2H, δ), 2.53 (t, *J* = 7.4 Hz, 2H, ζ), 2.30 (p, *J* = 6.1 Hz, 2H, β), 2.21 (p, *J* = 7.6 Hz, 2H, ε).

^{13}C NMR (126 MHz, chloroform-*d*): δ 173.6 (C_q) , 166.2 (C_q), 161.3 (C_q), 159.4 (C_q), 158.8 (C_q), 158.4 (C_q), 152.2 (C_q), 152.1 (1), 151.5 (C_q), 137.8 (19), 137.2 (3), 136.1 (22), 135.8 (C_q), 131.4 (C_q), 131.1 (16), 131.0 (25), 130.9 (C_q), 130.9 (15), 130.0 (C_q), 129.4 (17), 129.2 (23), 128.9 (C_q), 128.8 (C_q), 128.5 (18+24), 128.1 (C_q), 127.5 (7), 127.4 (6), 126.7 (11 + 12), 126.6 (2), 125.9 (9), 125.1 (C_q), 125.0 (C_q), 124.9 - 124.8 (8, 10, 13), 124.5 (4), 124.0 (26), 123.4 (14), 120.6 (21), 120.3 (22), 110.9 (5), 67.5 (α), 61.1 (γ), 33.9 (δ), 32.8 (ζ), 28.4 (β), 26.9 (ε).

LC-MS (MeOH): *m*/*z* (calc.) 970.3 (970.21, [**5**]$^+$), 488.2 (488.14, [**5** – Cl + MeCN]$^{2+}$), 700.2 (700.11, [**5** – 1-pyrenebutyric acid]$^+$), 741.2 (741.13, [**5** – 1-pyrenebutyric acid + MeCN]$^+$).

HRMS (MeOH): *m*/*z* (calc.) 970.20924 (970.20979, [**5**]$^+$), 467.62056 (467.62025, [**5** - Cl]$^{2+}$), 488.13395 (488.13359, [**5** – Cl + MeCN]$^{2+}$).

UV-vis: λ_{max} = 577 nm, ε = 9400 ± 500 $M^{-1}cm^{-1}$ in pure methanol.

Elem. Anal: Calcd (%). for [**5**]Cl: C, 66.86; H, 4.31; N, 6.96. Found: C, 66.81; H, 4.43; N, 6.92.

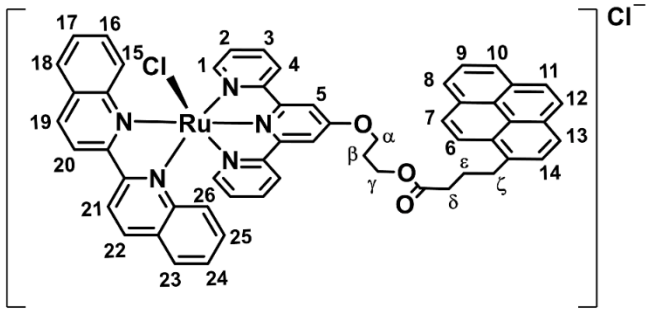

[Ru(biq)(**3**)(STF-31)]$(PF_6)_2$ ([**1**]$(PF_6)_2$)

[**1**]$(PF_6)_2$) was prepared according to a modified literature procedure.[1] [**5**]Cl (103 mg, 0.10 mmol) was dissolved in deoxygenated acetone/water 1:1 (15 ml) and STF-31 (83 mg, 0.20 mmol) was added. $AgPF_6$ was dissolved in deoxygenated acetone/water 1:1 (62 mg/ml) and 1.0 ml of this solution was added (0.25 mmol) to the reaction mixture. The mixture was heated to 50 °C under nitrogen, in the dark. After 3 h, the reaction mixture was filtered over Celite; the filter was flushed with acetone (3x 25 ml) to collect the product. Acetone was evaporated by rotary evaporation and the remaining water was decanted. The purple solid on the flask wall was washed with milliQ water (3 x 25 ml) and dried *in vacuo*. The crude mixture was separated on a silica column (acetone, then increase to acetone + 1% KPF_6 (sat.) with steps of + 0.25% KPF_6). The purple band with R_f = 0.31 in acetone + 2% KPF_6 (sat.) was collected and the solvent was rotary evaporated, then the solid was washed with MilliQ (3 x 25 ml) and dried *in vacuo* to obtain [**1**]$(PF_6)_2$ as a dark purple solid (134 mg, 0.081 mmol, 81%).

^{1}H NMR (500 MHz, acetone-*d*6): δ 9.56 (s, 1H, N1), 9.24 (d, *J* = 9.0 Hz, 1H, 20), 9.11 (d, *J* = 9.0 Hz, 1H, 19), 9.00 (d, *J* = 8.9 Hz, 1H, 21), 8.98 (d, *J* = 2.3 Hz, 1H, 27), 8.94 (d, *J* = 8.1 Hz, 1H, 4A), 8.78 (s, 1H, 5A), 8.52 (m, 2H, 22 + 4B), 8.44 (s, 1H, 5B), 8.42 (d, *J* = 8.2 Hz, 1H, 15), 8.38-8.33 (m, 2H, 14 + 1A), 8.21 (d, *J* = 7.7 Hz, 1H, 10), 8.17 (t, *J* = 7.7 Hz, 1H, 3A), 8.16 – 8.13 (m, 2H, 8 + 1B), 8.11 (d, *J* = 9.3 Hz, 1H, 13), 8.07 (d, *J* = 7.7 Hz, 1H, 7), 8.06 (d, *J* = 8.7 Hz, 1H, 11), 8.03- 7.96 (m, 3H, 12, 9, 3B), 7.86 (m, 2H, 23, 6), 7.81 – 7.74 (m, 3H, 33, 16), 7.73 – 7.67 (m, 3H, 31, 28), 7.62 (d, *J* = 5.6 Hz, 1H, 30), 7.58 (d, *J* = 8.8 Hz, 2H, 34), 7.55 (7, *J* = 6.6 Hz, 1H, 2A), 7.51 (m, 2H, 18 + 2B), 7.47 – 7.41 (m, 3H, 24 + 32), 7.41 – 7.35 (m, 2H, 17, 25), 7.07 – 6.99 (m, 2H, 26 + N2), 6.97 (t, *J* = 7.1 Hz, 1H, 29), 4.70 (t, *J* = 6.2 Hz, 2H, α), 4.39 (t, *J* = 6.2 Hz, 2H, γ), 4.19 (d, *J* = 6.6 Hz, 2H, η), 3.38 (t, *J* = 7.6 Hz, 2H, δ), 2.52 (t, *J* = 7.2 Hz, 2H, ζ), 2.35 (p, *J* = 6.2 Hz, 2H, β), 2.13 (p, *J* = 8.5 Hz, 2H, ε), 1.32 (s, 9H, θ).

^{13}C NMR (126 MHz, acetone-*d*6): δ 173.7 (C_q), 168.0 (C_q), 166.3 (C_q), 161.6 (C_q), 160.6 (C_q), 159.9 (C_q), 159.4 (C_q), 159.2 (C_q), 156.8 (C_q), 155.3 (1A), 153.7 (1B), 151.9 (C_q), 151.1 (C_q), 148.5 (30), 143.8 (C_q), 142.9 (27), 140.1 (19), 139.8 (3B), 139.6 (3A), 139.4 (22), 139.1 (C_q), 138.7 (C_q), 137.1 (C_q), 133.5 (C_q), 132.4 (25), 132.3 (C_q), 132.0 (17), 131.8 (C_q), 131.2 (C_q), 130.9 (15), 130.8 (C_q), 130.4 (23), 130.0 (16), 129.6 (24+2B), 129.5 (C_q), 129.4 (2A), 129.3 (28), 128.7 (32), 128.5 (31), 128.4 (6), 128.4 (12), 128.2 (13), 127.6 (33), 127.6 (18), 127.6 (11), 126.9 (9), 126.9 (34), 126.6 (4A), 126.6 (29), 125.9 (10), 125.8 (7), 125.7 (8), 125.7 (C_q), 125.4

(4B), 124.8 (26), 124.3 (14), 122.3 (20), 122.1 (21), 113.3 (5A), 112.6 (5B), 67.9 (α), 61.4 (γ), 47.1 (η), 34.2 (ζ), 33.2 (δ), 31.3 (θ), 29.1 (β), 27.8 (ε).

LC-MS (MeOH): *m*/*z* (calc.) 679.1 (679.3, [**1**]$^{2+}$), 1357.6 (1357.6, [**1**-H]$^{+}$), 1503.6 (1503.6, [**1**+PF_6]$^{+}$).

HRMS (MeOH): *m*/*z* (calc.) 679.20118 (679.20163, [**1**]$^{2+}$).

UV-vis: λ_{max} = 537 nm, ε = 10700 ± 500 $M^{-1}cm^{-1}$ in pure methanol.

Elem. Anal: Calcd (%). for [**1**]$(PF_6)_2$: C, 57.56; H, 4.16; N, 6.80. Found: C, 57.06; H, 4.22; N, 6.73.

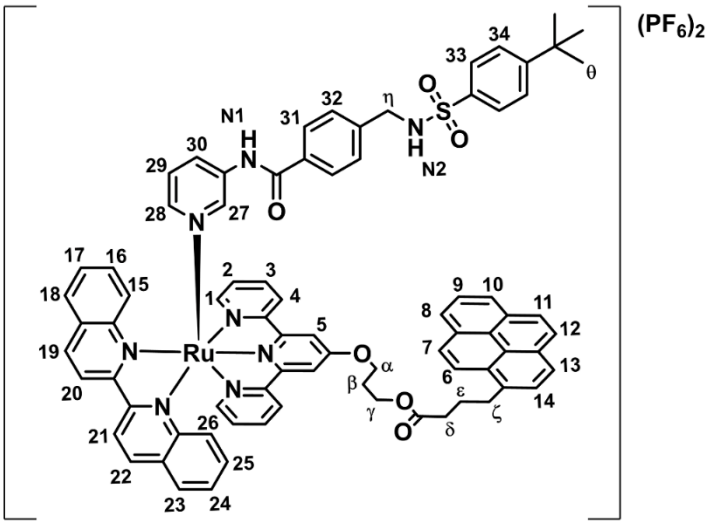

Ruthenium dimer [Ru(**2**)Cl_2]$_2$ ([**6**])

Compound [**6**] was prepared according to a modified literature procedure.[4] In a 3-neck round bottom flask equipped with drop funnel and nitrogen flow, [Ru_2Cl_2(*p*-cymene)$_2$] (431 mg, 0.70 mmol) was dissolved in deoxygenated DCM (25 ml). A solution of **2** (430 mg, 1.4 mmol) in deoxygenated DCM (25 ml) was transferred to the drop funnel, and added to the mixture over 60 minutes at RT. Once a dark purple color was obtained, the reaction mixture was filtered through a membrane filter and [**6**] was obtained as a purple solid (620 mg, 0.65 mmol, 92%).

^{1}H NMR (400 MHz, DMSO-d_6): δ (ppm) 9.35 (d, *J* = 5.4 Hz, 4H, 4), 8.63 (d, *J* = 6.1 Hz, 4H, 1), 8.35 (s, 4H, 5), 7.96 (t, *J* = 7.8 Hz, 4H, 2), 7.49 (t, *J* = 7.3 Hz, 4H, 3), 4.73 (t, *J* = 5.1 Hz, 2H, OH), 4.50 (t, *J* = 6.3 Hz, 4H, α), 3.67 (q, *J* = 5.9 Hz, 4H, γ), 2.03 (p, *J* = 6.2 Hz, 4H, β).

^{13}C NMR (101 MHz, DMSO-d_6): δ (ppm) 166.4 (C_q), 159.0 (C_q), 157.6 (C_q), 156.0 (4), 136.7 (2), 126.3 (3), 123.3 (1), 108.8 (5), 66.7 (α), 57.1 (γ), 31.9 (β).

LCMS (MeOH): *m*/*z* (calc.) 599.9 (600.03 [Ru(**2**)Cl(DMSO)$_2$]$^{+}$).

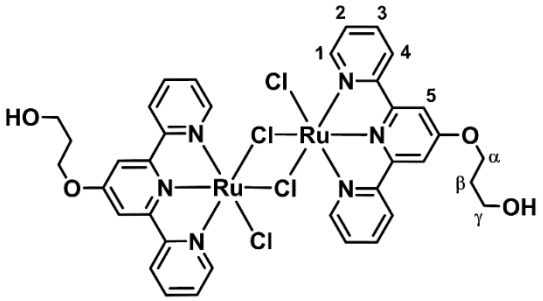

[Ru(biq)(**2**)Cl]Cl ([**7**]Cl)

[**7**]Cl was prepared according to a modified literature procedure.[1] Dimer [**6**] (540 mg, 0.56 mmol) was dissolved in deoxygenated ethylene glycol (7 ml) and 2,2′-biquinoline (292 mg, 1.14 mmol) was added. The mixture was heated up to 180 °C under a nitrogen atmosphere. After 2.5 h, the reaction mixture was diluted with ethanol (10 ml), and filtered over Celite to remove insoluble impurities. Ethanol was removed by rotary evaporation and the crude was purified over an alumina oxide column (DCM, gradual increase to 92:8 DCM/MeOH) to remove ethylene glycol. The obtained dark purple/blue solid was dried *in vacuo* to yield [**7**]Cl (250 mg, 0.34 mmol, 30%).

^{1}H NMR (400 MHz, methanol-d_4): δ (ppm) 9.60 (d, J = 0.9 Hz, 1H, 15), 8.91 (d, J = 8.9 Hz, 1H, 20), 8.83 (d, J = 8.3 Hz, 1H, 19), 8.62 (d, J = 8.8 Hz, 1H, 21), 8.45 (d, J = 8.1 Hz, 2H, 4), 8.28 (s, 2H, 5), 8.25 (d, 8.2 Hz, 1H, 18), 8.19 (d, 1H, 22), 7.89 – 7.74 (m, 7H, 3, 16, 16, 23, 1), 7.43 (t, J = 8.1 Hz, 1H, 24), 7.30 – 7.23 (m, 3H, 25, 2), 6.89 (d, J = 8.9 Hz, 1H, 26), 4.56 (t, J = 6.2 Hz, 2H, α), 3.88 (t, J = 6.1 Hz, 2H, γ), 2.19 (p, J = 6.2 Hz, 2H, β).

^{13}C NMR (101 MHz, methanol-d_4): δ 168.1 (C_q), 163.4 (C_q), 160.9 (C_q), 160.5 (C_q), 160.3 (C_q), 154.0 (1), 153.4 (C_q), 152.7 (C_q), 139.6 (19), 138.7 (3), 137.3 (22), 132.0 (16), 131.7 (25), 130.6 (C_q), 130.4 (23), 130.4 (17), 129.9 (18), 129.7 (C_q), 129.6 (24), 128.2 (2), 125.1 (4, 26), 121.7 (21, 22), 111.9 (5), 70.5 (α), 62.3 (γ), 32.7 (β).

LCMS (MeOH): m/z (calc.) 700.7 (700.1, [**7**]$^+$), 352.2 (353.1, [**7** – Cl + MeCN]$^{2+}$).
HRMS (MeOH): m/z (calc.) 700.10414 (700.10485, [**7**]$^+$), 353.08095 (353.08105, [**7** – Cl + MeCN]$^{2+}$), 332.56763 (332.56774, [**7** – Cl]$^{2+}$).

UV-vis: λ_{max} = 577 nm, ε = 9200 ± 200 $M^{-1}\cdot cm^{-1}$ in pure methanol.

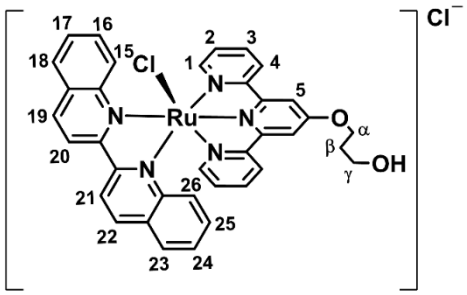

[Ru(biq)(**2**)(STF-31)](PF$_6$)$_2$ ([**8**](PF$_6$)$_2$)

[**8**](PF$_6$)$_2$) was prepared according to a modified literature procedure.[1] [**7**]Cl (50 mg, 0.07 mmol) was dissolved in deoxygenated acetone/water 1:1 (7 ml) and STF-31 (43 mg, 0.14 mmol) was added. AgPF$_6$ was dissolved in deoxygenated acetone/water 1:1 (212 mg/ml) and 100 µL of this solution (0.08 mmol AgPF$_6$) was added to the reaction mixture. The mixture was heated to 50 °C under nitrogen, in the dark. After 3 h, the reaction mixture was filtered over Celite; the filter was flushed with acetone (3 x 25 ml) to collect the product. Acetone was rotary evaporated and the remaining water was decanted. The purple solid on the flask wall was washed with MilliQ water (3 x 25 ml) and dried *in vacuo*. The crude was separated on a silica column (acetone, then increase to acetone + 0.5% KPF$_6$ (sat.) with steps of + 0.25% KPF$_6$). The purple band with R_f = 0.16 in acetone + 2% KPF$_6$ (sat.) was collected and the solvent was evaporated, then washed with MilliQ (3 x 25 ml) and dried *in vacuo* to obtain [**8**](PF$_6$)$_2$ as a dark purple solid (4 mg, 0.003 mmol, 4%).

^{1}H NMR (500 MHz, acetone-*d*6) δ 9.65 (s, 1H, N1), 9.25 (d, *J* = 8.9 Hz, 1H, 20), 9.12 (d, *J* = 8.8 Hz, 1H, 19), 9.05 – 8.97 (m, 3H, 21, 27, 4A), 8.79 (s, 1H, 5A), 8.61-8.56 (m, 2H, 22, 4B), 8.46 – 8.40 (m, 2H, 5B, 15), 8.37 (d, *J* = 5.6 Hz, 1H, 1A), 8.23 (t, *J* = 7.8 Hz, 1H, 3A), 8.16 (d, *J* = 5.5 Hz, 1H, 1B), 8.06 (t, *J* = 7.9 Hz, 1H, 3B), 7.99 (d, *J* = 8.1 Hz, 1H, 23), 7.82 – 7.76 (m, 4H, 16, 28, 33), 7.73 (d, *J* = 8.1 Hz, 2H, 31), 7.66 (d, *J* = 5.7 Hz, 1H, 30), 7.63 – 7.50 (m, 5H, 34, 24, 18, 2A, 2B), 7.50 – 7.40 (m, 4H, 25, 32, 17), 7.11 – 7.01 (m, 3H, 26, N2, 29), 4.69 (t, *J* = 6.4 Hz, 2H, α), 4.20 (d, *J* = 6.6 Hz, 2H, η), 3.88 (t, *J* = 5.0 Hz, 1H, OH), 3.83 (q, *J* = 5.6 Hz, 2H, γ), 2.18 (p, *J* = 6.3 Hz, 2H, β), 1.34 (s, 9H, θ).

^{13}C NMR (126 MHz, acetone-*d*6) δ 168.2 (C$_q$), 166.4 (C$_q$), 161.6 (C$_q$), 160.6 (C$_q$), 156.8 (C$_q$), 155.4 (1A), 153.7 (1B), 152.0 (C$_q$), 151.1 (C$_q$), 148.6 (30), 143.8 (C$_q$), 142.9 (27), 140.0 (19), 139.8 (3A), 139.6 (3B), 139.4 (22), 139.1 (C$_q$), 138.7 (C$_q$), 133.5 (C$_q$), 132.5 (17), 132.0 (25), 131.1 (C$_q$), 130.9 (15), 130.5 (23), 130.0 (16), 129.7 (28), 129.6 (C$_q$), 129.6 (2A + 2B), 129.3 (24), 128.7 (32), 128.5 (31), 127.6 (33+18), 126.9 (34), 126.7 (4A) 126.6 (29), 125.3 (4B), 124.9 (26), 122.3 (20), 122.1 (21), 113.2 (5A), 112.6 (5B), 68.3 (α), 58.5 (γ), 47.1 (η), 32.8 (θ).

LC-MS (MeOH): *m*/*z* (calc.) 544.0 (544.1, [**8**]$^{2+}$), 1087.6 (1087.3, [**8**-H]$^+$), 1233.6 (1233.2, [**8**+PF$_6$]$^+$).

HRMS (MeOH): *m*/*z* (calc.) 544.14840 (544.14895, [**8**]$^{2+}$).

UV-vis: λ_{max} = 538 nm, ε = 9000 ± 600 M^{-1}cm^{-1} in pure methanol.

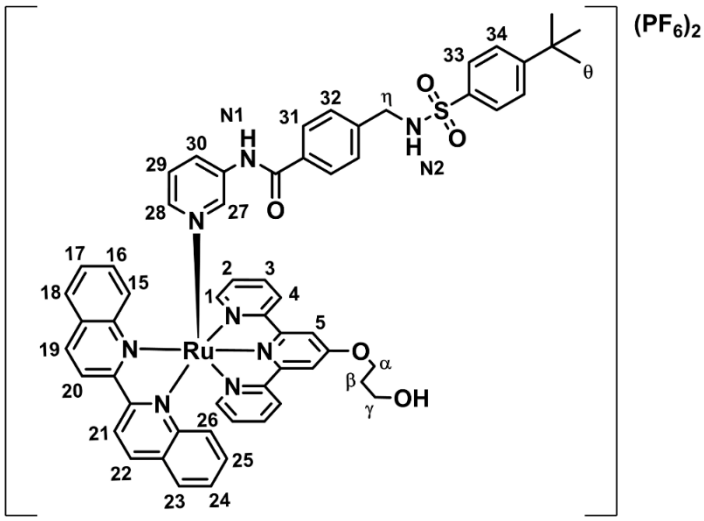

Photochemistry

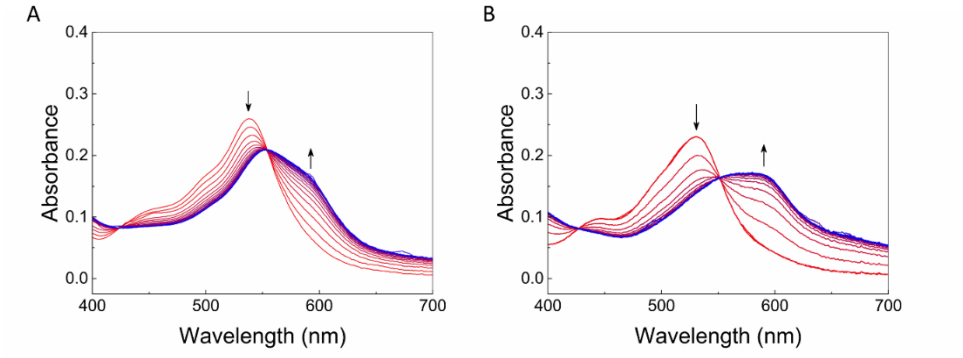

Figure S7.1: Evolution of the absorption spectrum of a solution of [**8**](PF$_6$)$_2$ and [**9**](PF$_6$)$_2$ (respectively A and B, 25 μM) in methanol upon irradiation with 530 nm light (photon flux = 1.36 x 10^{-7} mol·s^{-1}). Spectra shown between t = 0 minutes (red spectrum) and t = 10 minutes (blue spectrum). Spectra were recorded under air, every 30 seconds. Temperature: 298 K.

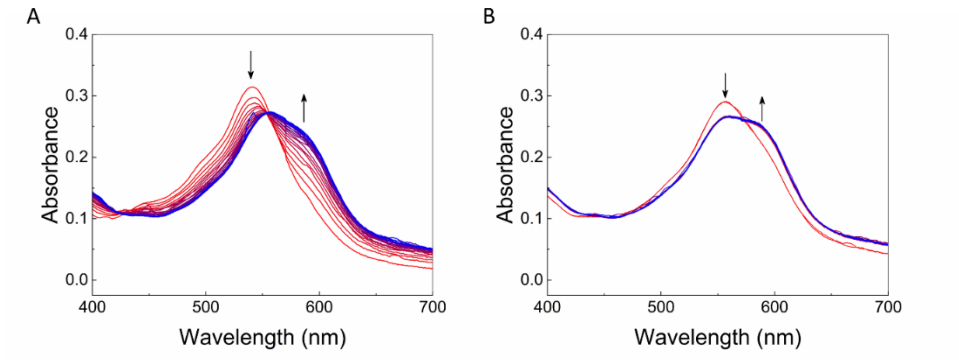

Figure S7.2: Evolution of absorbance for a solution of [**1**](PF$_6$)$_2$ (25 μM) in methanol/water (95:5) upon 1st (A) and 2nd (B) irradiation with 530 nm light (photon flux = 1.36 x 10^{-7} mol·s^{-1}). Spectra shown between t = 0 minutes (red spectrum) and t = 10 minutes (blue spectrum). Spectra were recorded under air, every 30 seconds. Temperature: 298 K.

2D luminescence plots

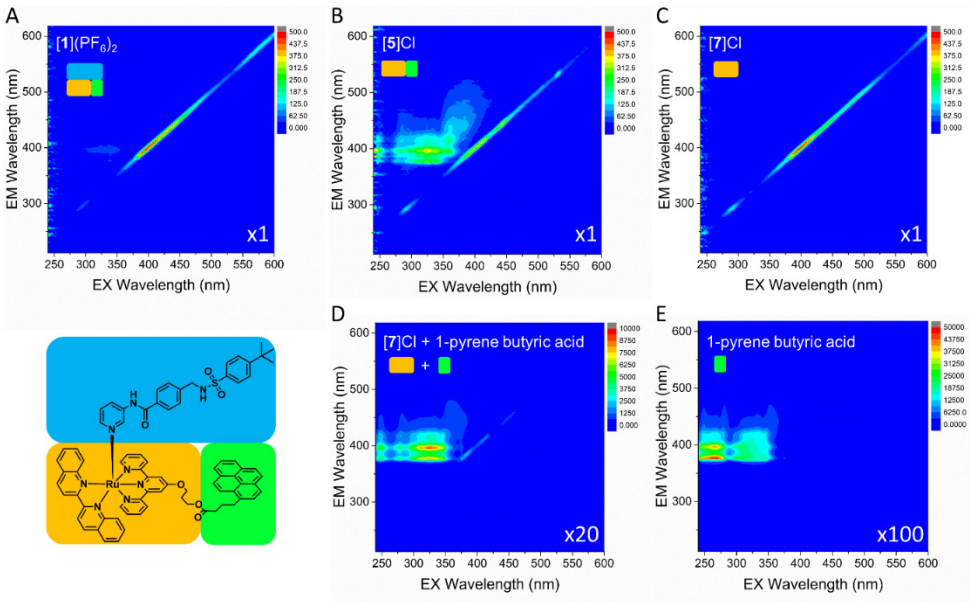

Figure S7.3: 2D Luminescence plots of [**1**](PF$_6$)$_2$, [**5**]Cl, [**7**]Cl, [**7**]Cl + 1-pyrene butyric acid and 1-pyrene butyric acid (respectively A-E, 50 μM) in methanol. Compounds are schematically represented by the components of the intact complex as orange, green and blue boxes. Excitation (EX) wavelength is plotted on the x-axis and emission (EM) wavelength on the y-axis. Rainbow color scale shows relative fluorescence intensity, with red for high emission and blue for no emission. Scale multiplier is indicated by the number in the bottom right of each panel. Detections at EX = EM are due to scattering of the excitation laser by the solutions.

Förster distance and FRET efficiency

The Förster distance R_0 in Å, at which 50% of the fluorescence of the donor (here: 1-pyrenebutyric acid) is quenched by the acceptor (here: **[8]**$(PF_6)_2$) was calculated using Eq. 1:[5]

$$R_0 = 9.78\ x\ 10^3\ (k^2 n^{-4} \varphi_D\ J_{DA})^{1/6} \qquad \text{(Eq. 1)}$$

Where k^2 is the orientation factor (k^2 = 2/3), n is the refractive index of the solution (n = 1.33 for methanol), and φ_D is the emission quantum yield from the donor (φ_D = 0.067 for 1-pyrenebutyric acid in methanol[6]). Using Eq. 2, we calculated J_{DA} in $M^{-1}cm^3$, *i.e.* the spectral overlap of $F_D(\lambda)$, which is the emission intensity of the donor at wavelength λ, with the total area of the emission spectrum normalized to 1 (dimensionless), and ε_A in $M^{-1}cm^{-1}$, which is the extinction coefficient of the acceptor, multiplied by λ^4 (with λ in cm). For a plot of J_{DA} *vs.* λ, see Figure S7.4A.

$$J_{DA} = \int F_D(\lambda)\varepsilon_A(\lambda)\lambda^4 d\lambda \qquad \text{(Eq. 2)}$$

For J_{DA} we found a value of 1.61 x 10^{-14} $M^{-1}cm^3$, giving R_0 = 24.4 Å for the pair 1-pyrenebutyric acid/**[8]**$(PF_6)_2$. We calculated the FRET efficiency φ_{FRET} using Eq. 3:[5]

$$\varphi_{FRET} = 1/(1 + (r/R_0)^6) \qquad \text{(Eq. 3)}$$

Using r = 20 Å (see Figure S7.4B), we found that φ_{FRET} = 0.77 for the donor/acceptor pair 1-pyrenebutyric acid/**[8]**$(PF_6)_2$ in methanol.

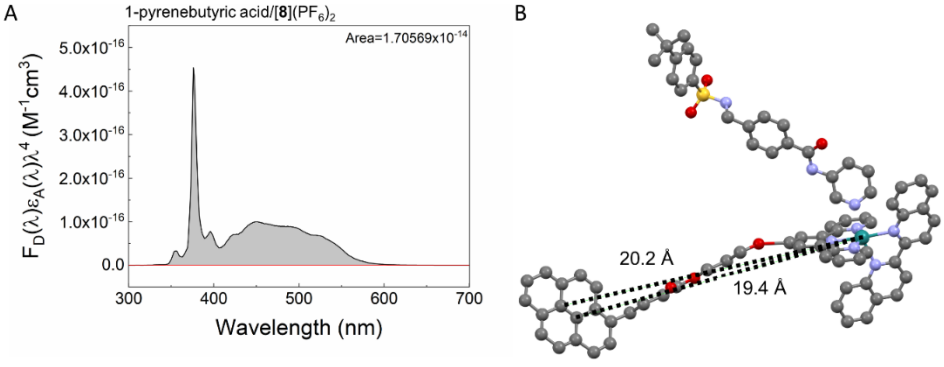

Figure S7.4: A) Spectral overlap ($\boldsymbol{F_D(\lambda)\varepsilon_A(\lambda)\lambda^4}$) of the emission intensity, total area normalized to 1, (F_D (λ)) of the donor 1-pyrenebutyric acid, and the extinction coefficient of the acceptor **[7]**Cl ε_A, multiplied by λ^4, *vs.* the wavelength (λ). B) Yasara simulation of $[\mathbf{1}]^{2+}$, the Ru-pyrene distance r (from the ruthenium ion to the center carbon atoms of the pyrene moiety) is indicated by the dashed lines; r was found to be 20 Å.

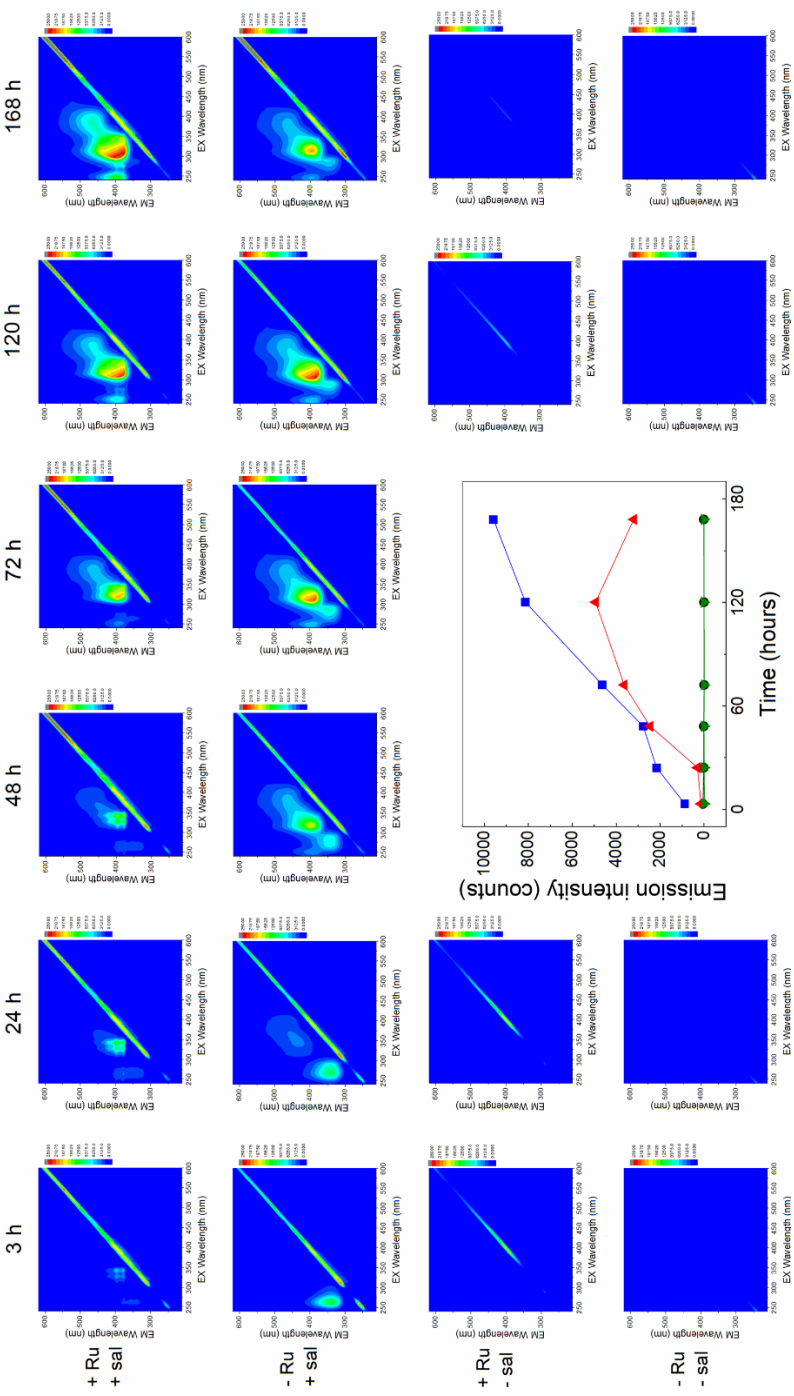

Figure S7.5: 2D emission spectra for [5]Cl degradation by saliva. Plus (+) or minus (–) on the far left indicates if the complex (Ru) and/or saliva (sal) are present in the sample ($[Ru]_{stock}$ = 1 mM, Ru/saliva = 1:19, when Ru or sal were not in the sample, they were replaced by MilliQ water). Color scale is the same for each panel (blue to red: 0 to 25000). Inset: emission intensity *vs.* time, excited at 354 nm, for +Ru/+sal (blue), –Ru/+sal (red), +Ru/–sal (black) and –Ru/+sal (green). Samples were incubated at 37 °C under stirring between measurements. Samples were centrifuged before measuring, emission was measured of the supernatant.

References

[1] L. N. Lameijer, D. Ernst, S. L. Hopkins, M. S. Meijer, S. H. C. Askes, S. E. Le Dévédec, S. Bonnet, *Angew. Chem., Int. Ed.* **2017**, *56*, 11549.

[2] U. Sampath, W. C. Putnam, T. A. Osiek, S. Touami, J. Xie, D. Cohen, A. Cagnolini, P. Droege, D. Klug, C. L. Barnes, A. Modak, J. K. Bashkin, S. S. Jurisson, *J. Chem. Soc., Dalton Trans.* **1999**, 2049.

[3] M. A. Furrer, F. Schmitt, M. Wiederkehr, L. Juillerat-Jeanneret, B. Therrien, *Dalton Trans.* **2012**, *41*, 7201.

[4] D. C. Marelius, S. Bhagan, D. J. Charboneau, K. M. Schroeder, J. M. Kamdar, A. R. McGettigan, B. J. Freeman, C. E. Moore, A. L. Rheingold, A. L. Cooksy, D. K. Smith, J. J. Paul, E. T. Papish, D. B. Grotjahn, *Eur. J. Inorg. Chem.* **2014**, *2014*, 676.

[5] A. Bahreman, J.-A. Cuello-Garibo, S. Bonnet, *Dalton Trans.* **2014**, *43*, 4494.

[6] Y. Matsushita, M. Tsukiori, T. Suzuki, I. Moriguchi, *J. Pharm. Sci.* **1986**, *75*, 193.